DEUTSCHES ELEKTRONEN-SYNCHROTRON

DESY 94-016
February 1994

The Triple Regge Limit of Diffractive Dissociation in Deep Inelastic Scattering

J. Bartels, M. Wüsthoff

II. Institut für Theoretische Physik, Universität Hamburg

ISSN 0418-9833

NOTKESTRASSE 85 - 22603 HAMBURG

To be sure that your preprints are promptly included in the HIGH ENERGY PHYSICS INDEX, send them to (if possible by air mail):

DESY **Bibliothek** **Notkestraße 85** **22603 Hamburg** **Germany**	**DESY-IfH** **Bibliothek** **Platanenallee 6** **15738 Zeuthen** **Germany**

DESY 94-016
February 1994

ISSN 0418-9833

The Triple Regge Limit of Diffractive Dissociation in Deep Inelastic Scattering

J. Bartels
II. Institut für Theoretische Physik, Universität Hamburg
and
M. Wüsthoff
II. Institut für Theoretische Physik, Universität Hamburg

Abstract: We derive, within perturbative QCD, a formula for the inclusive cross section of the diffractive dissociation of the deep inelastic photon $\gamma + q \to X + q$ in the triple Regge limit $s \gg M^2 \gg Q^2 \gg \Lambda^2$. We use the leading $\ln(s/M^2)$, $\ln(M^2/Q^2)$ approximation and derive an expression for the triple Pomeron vertex. The Pomeron above this vertex is found to be of higher order than the BFKL Pomeron. We show that the Abramovsky-Gribov-Kanchelli cutting rules are satisfied, and we discuss implications for the Pomeron structure function.

1 Introduction

Recent interest in the low-x region of deep inelastic scattering (DIS) reminds us that the high-energy behaviour of QCD in the Regge limit is still unknown. Because of its non-perturbative nature, it has been believed for a long time that perturbation theory cannot be of much help. The low-x limit of DIS, however, has brought a new element into this discussion: taking $x_{Bjorken} \to 0$ at fixed Q^2 is the same as the Regge limit of the elastic scattering $(virtual)\ \gamma + p \to (virtual)\ \gamma + p$, and, at least for sufficiently large Q^2 there is a region in $x_{Bjorken}$ where perturbation theory rests on a very solid basis. Starting from this "allowed" region, one can try to go down in $x_{Bjorken}$ and Q^2 and study how more and more perturbative corrections to the leading approximation become important and, eventually, signal the breakdown of perturbation theory. In other words, the low-x region of DIS seems to provide, for the first time, a "perturbative entry" into the Regge regime. This is why in the discussion of low-x physics so many terms of "old-fashioned" Regge-physics reappear. The most prominent example is the so-called BFKL-*Pomeron* which recently has been found very useful in describing the rise of F_2 at small x [1, 2].

One of the key quantities in a Regge-analysis beyond the leading-pole approximation is the triple-Pomeron vertex. In hadron-hadron scattering it appears, for example, in the inclusive cross section $p + p \to anything + p$ in the triple-Regge limit $s \gg M^2 \gg 1GeV^2$ (M being the invariant mass of " anything"). Its numerical value has been extracted from fits to experimental data. In DIS, the analogue of this process is the diffractive dissociation of the photon, i.e. $\gamma + p \to anything + p$, and it is the virtuality Q^2 of the photon which, when chosen to be large enough, legitimates the use of perturbation theory. In the formula for the cross section one expects to see the perturbative approximation for the triple Pomeron vertex: in view of its importance in the (nonperturbative) Regge limit, a detailed analysis of the perturbative analogue may meet some interest. As the main result, we show that the triple Regge cross section consists of two BFKL Pomerons which merge into a "higher order" Pomeron. The latter one contains both four gluon and two gluon t-channel states and, hence, is more complex than the BFKL Pomeron. As a result, the triple Pomeron vertex is not simply a coupling between three BFKL Pomerons. Apart from the theoretical interest, this process also seems to be of practical relevance for HERA: both ZEUS and H1 [3, 4] have seen "diffractive-like" events which are not described by standard DIS Monte Carlos and, hence, seem to present some sort of corrections to the standard deep-inelastic framework.

In this paper we present the results of a perturbative analysis of the diffractive dissociation of the (virtual) photon in the triple Regge limit. First steps in this direction have been carried out before in [5, 6, 7, 8]: these calculation use the "hard scattering" approach, i.e. the leading-log Q^2 approximation (with the exception of [6, 7], these studies work even in the double-logarithmic approximation). In contrast to this, we shall work in the leading-log $1/x$ (but all orders in $\log Q^2$) approximation which is completely analogous to the derivation of the BFKL-Pomeron. In [9] this approximation has been used to derive the first "unitarity"

corrections to the BFKL-Pomeron; here we shall calculate, in the same spirit, the inclusive cross section of diffractive dissociation. As the main result, we obtain an expression for the triple-Pomeron vertex. After integration over M^2, our result coincides with that of [9].

A few words should be said about the technique used in this paper. We start from individual Feynman diagrams, using a physical gauge and performing the appropriate high energy approximations. However, we shall illustrate that, even in lowest order α_s, it is more economic to use the technique of dispersion relations introduced in [9]. In fact, when adressing higher order corrections we see no alternative to this technique.

Our paper is organized as follows. We start with the lowest order diagrams, the closed fermion loop with four gluons. Next we consider the order-α_s corrections and derive the expression for the triple-Pomeron vertex. In the third part we generalize this result to all orders in α_s. In the following section we discuss the validity of the Abramovsky-Gribov-Kanchelli cutting rules [10]. The final section contains a short summary and discussion of our results.

2 The Fermion loop

As we have said in the introduction the process of interest is the diffractive dissociation of the photon in the triple Regge region. To be more precise, we consider the process [1] (Fig.2.1) $(virtual)\ \gamma + q \to q\bar{q} + n\,gluons + q$ in the limit where the total energy $s \gg M^2 \gg Q^2 \gg \Lambda^2$ and $t \approx 0$ (Q^2 is the mass of the virtual photon, M the invariant mass of the $q\bar{q} - n\,gluon$ system, t the momentum transfer of the lower quark, and the lower t-channel carries color quantum number zero). It may be useful to remember that the cross section for this process is obtained from the $3 \to 3$ process illustrated in Fig.2.2 which allows for the following integral representation:

$$\begin{aligned} T_{3\to 3} &= \frac{s_1 s_2}{M^2} \int \frac{dj}{2\pi i} \int \frac{dj_1}{2\pi i} \int \frac{dj_2}{2\pi i} \left(\frac{s_1}{M^2}\right)^{j_1 - 1} \left(\frac{s_2}{M^2}\right)^{j_2 - 1} \left(\frac{M^2}{Q^2}\right)^{j-1} \xi_{j_1} \xi_{j_2} \xi_{j\,j_1 j_2} \cdot \\ &\quad \cdot F(j, j_1, j_2, t, t_1, t_2) + ... \\ \xi_j &= -\pi \frac{e^{-i\pi j} + \tau}{sin\pi j} \\ \xi_{j;j_1 j_2} &= -\pi \frac{e^{-i\pi(j - j_1 - j_2)} + \tau\tau_1\tau_2}{sin\pi(j - j_1 - j_2)} \end{aligned} \tag{2.1}$$

(the dots indicate that, in general, this amplitude has more terms which belong to other sets of energy discontinuities: none of them, however, contributes to the discontinuity in M^2; $M^2 = (p_{a_1}^2 + p_{b_1}^2 - p_{c_1}^2)^2$ according to the notation of Fig. 2.2). To obtain the cross section we are interested in, we put $s_1 = s_2 = s$, $t = 0, t_1 = t_2 = t$, take the discontinuity in M^2 and

[1] Strictly speaking this process is somewhat oversimplified: the quark at the bottom should be replaced by a colorless object. This defect will manifest itself in a divergence of the transverse momentum integral of the lowest cell on each side. We shall ignore this divergence by simply not carrying out this last integral.

replace the second signature factor by its complex conjugate:

$$\frac{d^2\sigma}{dt dM^2} = \frac{1}{16\pi M^2} \int \frac{dj}{2\pi i} \int \frac{dj_1}{2\pi i} \int \frac{dj_2}{2\pi i} \left(\frac{s}{M^2}\right)^{j_1 + j_2 - 2} \left(\frac{M^2}{Q^2}\right)^{j-1} \xi_{j_1} \xi^*_{j_2} F(j, j_1, j_2, 0, t, t) \tag{2.2}$$

The three angular momentum variables are independent of each other. Sometimes it will be convenient to perform the integration over the invariant mass: this gives a pole factor $1/(j - j_1 - j_2 + 1)$ which leads to the conservation of "reggeon energies" $j - 1 = j_1 - 1 + j_2 - 1$. Throughout our paper we shall make use of Sudakov variables [11]. We work in a frame where the photon momentum q and the momentum p of the incoming quark are along the z-direction. We neglect quark masses and take p^2 to be zero. Since the photon is off-mass shell we construct a second light-like momentum vector Q' as the linear combination of Q and p ($Q' = Q + xp$). The four-dimensional Minkowski space is now represented in terms of Q', p and a remaining transverse subplane (transverse to both Q' and p). The momentum k of Fig. 2.3, for example, can be written as $k = \alpha_k Q' + \beta_k p + k_t$. In the large-s limit (which is the same as the limit $x = Q^2/s \to 0$ limit) only the leading behaviour in $s = 2pQ'$ will be kept. This allows us to restrict ourselves to the polarization of the virtual gluon along the quark momentumg p. For the purpose of this paper it will be sufficient to concentrate on the transverse polarization of the virtual photon (which corresponds to the transverse part of the deep inelastic cross-section). Formulas for the longitudinal part can be derived in a similar way.

The lowest order diagrams are given by the process $\gamma + q \to q\bar{q} + q$ (Fig.2.3); in the corresponding cross section the main ingredient is the fermion loop with four t-channel gluons attached to it in all possible ways. This subamplitude has been studied in [8, 12], but we need a few properties which have not been discussed before. Before we start the analysis of this amplitude we find it even useful to recapitulate the simpler case of the two-gluon amplitude. To this end we have to consider the same process $\gamma + q \to q\bar{q} + q$, but only the single gluon exchange as is usually considered in the case of inclusive deep inelastic scattering. The lowest order diagrams are shown in Fig.2.4.a. As a subprocess, they contain the imaginary part of the elastic photon-gluon scattering amplitude (with both the photon and the gluon being off-shell). Calculations for this case are contained in [8, 12, 13, 14], and we can be brief. The square of the matrixelement (integrated over the transverse momentum of the quark pair) leads to the fermion-box (Fig.2.4.b) and its twisted counterpart (the third diagram of the closed fermion loop belongs to the left-hand cut in the invariant mass of the two-fermion system). We contract the hadronic tensor $\Phi^{\mu\nu}$, which represents the fermion-box according to the Feynman-rules, with $-g_{t_{\mu\nu}}$, i.e. we sum over the two orthogonal transverse polarizations of the virtual photon. Since the t-channel state is colourless, the colour of the two gluons has to be the same. The final (integrated over the transerse momentum of the quarks and the invariant mass M^2) result for the fermion-box (Fig. 2.4.b) is:

$$D^{a_1 a_2}_{(2,0)}(l) = \frac{1}{\sqrt{8}} \delta^{a_1 a_2} D_{(2;0)}(l) \tag{2.3}$$

with

$$D_{(2;0)}(l) = \sum_f \frac{e_f^2\alpha_s}{4\pi}\frac{\sqrt{8}}{2\pi}\int_0^1 d\alpha\int_0^1 dy\frac{[1-2\alpha(1-\alpha)][1-2y(1-y)]\,l^2}{y(1-y)l^2+\alpha(1-\alpha)} \qquad (2.4)$$
$$= \sum_f \frac{e_f^2\alpha_s}{4\pi}\frac{\sqrt{8}}{2\pi}\int_0^1 d\alpha\int_0^1 dy\frac{4\,\alpha^2y^2\,l^2}{y(1-y)l^2+\alpha(1-\alpha)}\ .$$

In this equation l denotes the transverse momentum of the virtual gluon [2], and l^2 is normalized with respect to Q^2, i.e., we substituted l^2/Q^2 by l^2. Throughout the paper all momenta will be normalized unless Q^2 is mentioned explicitly. The variable α coincides with the α_k in the Sudakov decomposition of k. The second integration variable y is a Feynman-parameter introduced in order to perform the k_t-integration. It may be worthwhile to note that the first (planar) box diagram in Fig.2.4.b serves as a subtraction for the transverse momentum integration. We have absorbed a factor $1/2\pi$, compensating a factor 2π which appears with the signature factor when we take the discontinuity of the diagrams (Fig.2.4.b), into $D_{(2;0)}$ [3]. In this way $D_{(2;0)}$ is normalized with respect to the partial wave F of the corresponding scattering amplitude. Another factor $1/(2\pi)$, belonging to the gluon loop below the fermion loop, has to be absorbed in the lower part of the diagrams in Fig. 2.4.b. This convention turns out to be convenient when higher order corrections will be considered: inside the gluon ladders, each loop comes with the phase-space integral $\int\frac{d^2l}{(2\pi)^3}$ and the two gluon propagators $1/(l^2)^2$. To complete this brief repeat of the two-gluon amplitude, we present the cross-section of the process shown in Fig.2.4.a:

$$\sigma(\gamma^*+q\to q\bar{q}+q) = \frac{\pi\,\alpha_{em}}{Q^2}\,4\pi\int\frac{d^2l}{(2\pi)^3}\,\frac{1}{l^4}\,D_{(2;0)}(l)\,\frac{\sqrt{2}}{3}\,g^2 \qquad (2.5)$$

The factor $\frac{\sqrt{2}}{3}\,g^2$ belongs to the lower part of the diagrams in Fig.2.4.b; as we have said before, the momentum l is normalized by Q. The infrared divergence in the l-integral reflects the fact that we are considering scattering of colored quarks. In order to obtain the unpolarized cross-section a factor $1/2$ has to be included. A factor $1/x$ which we did not absorbe into $D_{(2,0)}$ is combined with the flux-factor $1/(2s)$ leading to $1/(2Q^2)$ in the rhs. of eq. (2.5).

As an alternative to (2.4), one could have performed the α-integration using the δ-functions of the outgoing quark-lines and would then be left with a remaining integration over β: the leading logarithm in the limit $l^2\to 0$ then leads directly to the AP-splitting function for $g\to q\bar{q}$.

We now come back to the lowest order diffractive dissociation of the photon into two quarks (Fig.2.3). This process has been discussed also in [8, 5, 7, 12]. As long as the diffractive final state consists only of a $q\bar{q}$-system the triple Regge limit is not quite adequate: since the cross-section has large contributions in the region where M^2 is close to Q^2, we consider the region $s\gg M^2, Q^2\gg\Lambda^2$ (we shall return to the triple Regge limit as soon as the emission of gluons is included). In contrast to the previous case of the single-gluon exchange we now require color zero exchange between the lower quark and the $q\bar{q}$-system: as a consequence of this, we need at least two gluons in this t-channel. Although we are primarily interested in the diffractive dissociation, we shall, for completenes, also discuss the other possible quantum numbers of the two-gluon system. At the end of this section we will present an expression of the lowest order four-gluon amplitude $D_{(4;0)}$ which appears in the M^2-integrated cross section of the lowest order diffractive dissociation of the photon.

Let us begin with the first diagram of Fig.2.3 and its crossed counterpart (Fig.2.5). It is convenient to introduce the 4-vector $u=k_1+k_2$ and put $u^2=t=0$ which implies that u has only one component along p, i.e. $u=\beta_u p$. β_u itself is related to the invariant mass M of the two quarks ($M^2+Q^2=-\beta_u s$). The Regge limit forces $|\beta_u|$ to be small compared to 1. We restrict ourselves to the integration over β_{k_1} and α_{k_1} (or β_{k_2} and α_{k_2}) and keep the transverse momentum k_1 (k_2) fixed. The α_{k_1} integration can be done easily closing the contour of integration around the pole of the quark-propagator at the bottom of the diagrams. Absorbing the integral over β_{k_1} into the expression for the fermion pair, we obtain for the sum of the diagrams of Fig. 2.5:

$$\begin{aligned}
&\int_{\beta_u}^{1+\beta_u} d\beta_{k_2}\,\bar{u}(k-u)\,\hat{p}\,\frac{\hat{k}-\hat{k}_1}{(k-k_1)^2}\,\hat{p}\,\frac{\hat{k}}{k^2}\,\gamma_t^\mu\,v(q-k)\,T^bT^a\\
+&\int_{-1}^{\beta_u} d\beta_{k_1}\,\bar{u}(k-u)\,\hat{p}\,\frac{\hat{k}-\hat{k}_2}{(k-k_2)^2}\,\hat{p}\,\frac{\hat{k}}{k^2}\,\gamma_t^\mu\,v(q-k)\,T^aT^b\\
\simeq&\int_{\beta_u}^{1+\beta_u} d\beta_{k_2}\,\bar{u}(k-u)\,\hat{p}\,\frac{\hat{k}}{k^2}\,\gamma_t^\mu\,v(q-k)\,T^bT^a\,\frac{k\cdot p}{k\cdot k_2} \qquad (2.6)\\
+&\int_{-1}^{\beta_u} d\beta_{k_1}\,\bar{u}(k-u)\,\hat{p}\,\frac{\hat{k}}{k^2}\,\gamma_t^\mu\,v(q-k)\,T^aT^b\,\frac{k\cdot p}{k\cdot k_1}\\
=&\ \bar{u}(k-u)\,\hat{p}\,\frac{\hat{k}}{k^2}\,\gamma_t^\mu\,v(q-k)\,\left(T^bT^a\int_{\beta_u}^{1+\beta_u}\frac{d\beta_{k_2}}{\beta_{k_2}}+T^aT^b\int_{-1}^{\beta_u}\frac{d\beta_{k_1}}{\beta_{k_1}}\right)\\
\simeq&\ \bar{u}(k-u)\,\hat{p}\,\frac{\hat{k}}{k^2}\,\gamma_t^\mu\,v(q-k)\,\left[-T^bT^a\,\ln(\beta_u)+T^aT^b\,\ln(-\beta_u)\right]\ .
\end{aligned}$$

Here we have suppressed α_{k_1} and α_{k_2}: they are small compared to the other α-components. The limits of integration correspond to the physical subenergy s_1 ($s_1=-\beta_{k_1}s$, first diagram of Fig. 2.5) which has to be positive and smaller than s. This restricts β_{k_1} to lie in the intervall $(-1,0)$. The second contribution is a u-channel contribution ($u_2=-\beta_{k_2}s$, second diagram of Fig. 2.5) which has to be negative and larger than $M_X^2+Q^2-s$, i.e. β_{k_2} lies in the intervall $(0,1+\beta_u)$. The final result is

$$\bar{u}(k-u)\,\hat{p}\,\frac{\hat{k}}{k^2}\,\gamma_t^\mu\,v(q-k)\,\left\{\left[T^a,T^b\right]\,\ln(-\beta_u)+i\pi T^bT^a\right\}$$

[2] Our notation for the momenta is simplified in so far as we use the same letter for the 4-dimensional Lorentz-vector and its euclidean transverse and 2-dimensional component. In this way l^2 in eq.(2.4) has to be understood as l_t^2.

[3] The function $D_{(2;0)}$ is normalized in a slightly different way than in [9]: compared to that paper, we have an additional factor $\sqrt{8}/2\pi$.

$$= \bar{u}(k-u)\,\frac{\hat{k}}{k^2}\,\gamma_t^\mu\,v(q-k)\,\left\{-if^{abc}T^c\,\ln\left(\frac{s}{M_X^2+Q^2}\right)+i\pi T^bT^a\right\}\quad . \qquad (2.7)$$

The logarithm results from the integration over β_{k_1} and contributes to the real part of the amplitude. At this stage it is useful to introduce the signature $\tau = \pm$ of the two-gluon system: the amplitude is called to have positive (negative) signature, if it is symmetric (antisymmetric) under the combined exchange of color indices and momenta of the two gluon lines. It then follows from (2.7) that the (large) logarithm contributes only to negative signature $\tau = -$, where the two gluons are in the colour octet (8_A) state. This result is well known as the reggeization of the gluon [15]: apart from the logarithm, the first part of (2.7) coincides with the analogous part of Fig.2.4.a, i.e. the elementary gluon in Fig.2.4.a starts to turn into a reggeized gluon. Analyzing in the same way the other diagrams of Fig.2.3, we find that large logarithms can be obtained only from the first and the fourth diagram: in the other diagrams, one of the fermion propagators carries a large virtuality and thus prevents the formation of the logarithm. As a result, in the leading log(s) approximation the reggeized gluon couples to the fermion in the same way as the single gluon in Fig.2.4.a.

It remains to discuss the second part of (2.7), the imaginary part. It contains both even and and odd signature, and there is no restriction in color space: projection on the 8_A state with odd signature gives the (next-to leading) term of the reggeizing gluon, whereas the color singlet is what we have started out to obtain; the photon diffractive dissociation of the photon. In contrast to the logarithmic term, now all diagrams of Fig.2.3 are equally important.

To complete the discussion we restrict ourselves to the color singlet and present the cross-section for fixed M^2. For this we have to square the sum of diagrams in Fig.2.3 (see also [8]) and obtain:

$$\left.\frac{d\sigma^{DD}}{dt\,dM^2}(\gamma^*+q\to q\bar{q}+q)\right|_{t=0} = \sum_f e_f^2\,\frac{\alpha_{em}\pi^2\,\alpha_s^2}{24}\,\frac{1}{M^2}\int_0^1 d\alpha\,\left[\alpha^2+(1-\alpha)^2\right]\cdot \qquad (2.8)$$

$$\cdot\left\{\int\frac{dl^2}{l^4}\,\frac{4\alpha_s}{3\pi}\left[\frac{M^2-Q^2}{M^2+Q^2}+\frac{l^2+\alpha(1-\alpha)(Q^2-M^2)}{\sqrt{[l^2+\alpha(1-\alpha)(Q^2-M^2)]^2+4\alpha^2(1-\alpha)^2M^2Q^2}}\right]\right\}^2 .$$

In eq. (2.8) we put $l = k_1 = -k_2$, here not normalized by Q, and integrated over the azimuthangle of l. The divergence of the l-integral disappears, if we replace the quark at the lower end by a colourless particle.

We wish to point out that we could have obtained our result also in a slightly different way: rather than integrating over β_{k_1} and obtaining the logarithm, we could have started from an integral representation, analogous to (2.1), for the amplitude $\gamma + q \to q\bar{q} + q$ and calculated the discontinuity in s_1. Making use of the reggeization of the gluons (which here means the same as the use of a dispersion relation in s_1, with the subtraction constant being fixed by the Regge-signature factor) then would have told us what the real part in (2.7) has to be. This simple observation, in fact, illustrates that, in the Regge-limit under consideration,

the use of dispersion relations is a very economic way to calculate the high energy limit of multiparticle amplitudes. In the following we shall demonstrate this in more detail.

Let us then return to the cross section of the diffractive dissociation of the photon and rephrase our task: rather than calculating the square of the diagrams of Fig.2.3, we compute the triple energy discontinuity of the six-point amplitude (2.1), as illustrated in Fig.2.7. From the integral representation one sees that the triple energy discontinuity fixes the (real valued) partial wave amplitude F, and the signature factors then determine the phases. As we have said aleady after (2.1), our cross section is obtained by taking the single discontinuity in M^2 (and by replacing the second signature factor by its complex conjugate). A few advantages of this method can be seen immediately: between the cutting lines in Fig.2.7 we need to know only leading-order amplitudes: $\gamma + q \to q\bar{q} + q$ (see above), $q + q \to q + q$ etc. Furthermore, the results will be gauge-invariant since we are dealing with on-shell S-matrix elements. Alltogether, we have 16 terms, but using invariance under charge conjugation we are left with only 8 contributions. Between the gluon lines, all horizontal quark lines are on mass-shell, and we have enough δ- functions to do all β-integrations; in addition, we also integrate over the invariant mass M^2. It turns out that all gluons at one fermion line reggeize in the same way as in diagram Fig.2.6. We ignore the lower part of the diagram (i.e. the coupling of the gluons to the lower quark) and keep the transverse momenta of the gluons fixed. The eight terms for the fermion loop can be organized as illustrated in Fig.2.8: by adding and subtracting the last diagram one obtains seven combinations which have the same structure as Fig.2.4.b, namely the sum of a twisted and a non-twisted box. Consequently, we can use the result (2.4). Each of these seven combinations can be interpreted as the coupling of two reggeized gluons to two photons. As an example, in the first term, the gluons '2', '3', and '4' are parts of one reggeized gluon whereas gluon '1' is still elementary and will be reggeized in higher order.

Next, we have to analyse the colour contents of our diagrams: in all 8 diagrams we have traces over products of four tensors T^a in the fundamental (quark) colour representation where a denotes the color of one of the four gluons. Our previous discussion seems to suggest that we should form irreducible representations in the two subsystems (12) and (34) ($8 \otimes 8 = 1 \oplus 8_A \oplus 8_S \oplus 27 \oplus 10 \oplus \bar{10}$). This was done in [9]. However, for the moment we find it instructive to look for a colour decomposition which fits more closely the momentum structure. Very useful for our fermion loop calculation is the reduction of the quark-antiquark states into singlet and octet irreducible states as shown in Fig.2.10. Applying these relations we can rewrite the result of our four gluon amplitude at zero order in the following way:

$$\begin{aligned} D^{a_1a_2a_3a_4}_{(4,0)}(k_1,k_2,k_3,k_4) &= \frac{g^2}{2\sqrt{2}}\cdot \\ &\Big\{\, d^{a_1a_2a_3a_4}D_{(2;0)}(k_1,k_2+k_3+k_4) + d^{a_2a_1a_3a_4}D_{(2;0)}(k_2,k_1+k_3+k_4) \\ &+ d^{a_1a_2a_4a_3}D_{(2;0)}(k_3,k_1+k_2+k_4) + d^{a_1a_2a_3a_4}D_{(2;0)}(k_4,k_1+k_2+k_3) \\ &- \frac{1}{4}f^{a_1a_2c}f^{ca_3a_4}D_{(2;0)}(k_1+k_2,k_3+k_4) - \frac{1}{4}f^{a_1a_3c}f^{ca_2a_4}D_{(2;0)}(k_1+k_3,k_2+k_4) \end{aligned} \qquad (2.9)$$

$$
\begin{aligned}
&-\frac{1}{4}f^{a_1a_4c}f^{ca_2a_3}D_{(2;0)}(k_1+k_4,k_2+k_3)\\
&-\frac{1}{4}d^{a_1a_2c}d^{ca_3a_4}D_{(2;0)}(k_1+k_2,k_3+k_4)-\frac{1}{4}d^{a_1a_3c}d^{ca_2a_4}D_{(2;0)}(k_1+k_3,k_2+k_4)\\
&-\frac{1}{4}d^{a_1a_4c}d^{ca_2a_3}D_{(2;0)}(k_1+k_4,k_2+k_3)\\
&-\frac{1}{6}\delta^{a_1a_2}\delta^{a_3a_4}D_{(2;0)}(k_1+k_2,k_3+k_4)-\frac{1}{6}\delta^{a_1a_3}\delta^{a_2a_4}D_{(2;0)}(k_1+k_3,k_2+k_4)\\
&-\frac{1}{6}\delta^{a_1a_4}\delta^{a_2a_3}D_{(2;0)}(k_1+k_4,k_2+k_3)\Big\}\ .
\end{aligned}
$$

One has to remember that, taking the triple discontinuity, each of the three signature factors in eq. (2.1) gives a factor 2π. We, therefore, extract $(2\pi)^3$ from the diagram in Fig.2.7 and normalize, in this way, $D_{(4;0)}$ analoguous to F (see (2.1)). In order to apply the same rules as stated in connection with eq. (2.5) we absorb a factor $1/(2\pi)$ from each gluon loop below the fermion loop into the lower part of the diagram. Since we have expressed $D_{(4;0)}$ in terms of $D_{(2;0)}$ a colour factor $1/\sqrt{8}$, according to eq. (2.3), has to be added in (2.9). The tensor $d^{a_1a_2a_3a_4}$ is defined as follows (Fig.2.9):

$$
\begin{aligned}
d^{a_1a_2a_3a_4} &= Sp\{T^{a_1}T^{a_2}T^{a_3}T^{a_4}\}+Sp\{T^{a_4}T^{a_3}T^{a_2}T^{a_1}\}\\
&= -\frac{1}{4}f^{a_1a_2c}f^{ca_3a_4}+\frac{1}{4}d^{a_1a_2c}d^{ca_3a_4}+\frac{1}{6}\delta^{a_1a_2}\delta^{a_3a_4}\\
&= \frac{1}{4}f^{a_1a_4c}f^{ca_2a_3}+\frac{1}{4}d^{a_1a_4c}d^{ca_2a_3}+\frac{1}{6}\delta^{a_1a_4}\delta^{a_2a_3}
\end{aligned}
\qquad (2.10)
$$

The two possible decompositions of the tensor $d^{a_1a_2a_3a_4}$ (Fig.2.9) follow from the insertion of the irreducible $q\bar{q}$-states between the subsystem (12) and (34) or between (14) and (23). Both decompositions were used to derive the form (2.9). Fig.2.8 already suggests that all contributions to $D_{(4;0)}$ can be interpreted as reggeons, but beside the usual 8_A and odd-signature-reggeon we have the 8_S and even-signature-reggeons as well. The contributions with a pair of two odd-signature reggeons belong to the zero order fermion loop contribution of the Lipatov ladder. The last two lines of eq. (2.9) contain reggeon-like terms in the colour singlet state. Their ambiguous meaning will be discussed in the next section. The interpretation of a reggeon made up of two gluons is rather straightforward, but the reggeon composed of three gluons is more complicated. As fig.2.12 illustrates it can be decomposed in a reggeon and a single gluon. In any case it has the gluon-colour quantum numbers, but can be odd or even.

From the form (2.9) it is easy to find the irreducible representations of the subsystems (12) and (34). As an example, in order to obtain the color singlet amplitude which is relevant for the physical process of diffractive dissociation, we simply insert the colour singlet projector

$P_1^{(a_1a_2;a_3a_4)}=\frac{1}{8}\delta^{a_1a_2}\delta^{a_3a_4}$. The result is [4]:

$$
\begin{aligned}
&D_{(4,0)}^{(1;+,+)}(k_1,k_2,k_3,k_4) = g^2\,\frac{\sqrt{2}}{3}\ \cdot\\
&\Big\{\ D_{(2;0)}(k_1,k_2+k_3+k_4)+D_{(2;0)}(k_2,k_1+k_3+k_4)\\
&+D_{(2;0)}(k_3,k_1+k_2+k_4)+D_{(2;0)}(k_4,k_1+k_2+k_3)\\
&-D_{(2;0)}(k_1+k_2,k_3+k_4)-D_{(2;0)}(k_1+k_3,k_2+k_4)-D_{(2;0)}(k_1+k_4,k_2+k_3)\Big\}\ .
\end{aligned}
\qquad (2.11)
$$

The upper index $(1;+,+)$ means the colour singlet and even signature ($\tau=+$) state in the left and right subsystem. Remarkable properties of this result are the total symmetry under exchange of the momenta $k_1,...,k_4$ and its infrared behaviour: whenever one of the momenta k_i goes to zero the whole amplitude vanishes. This reflects the colour-gauge-cancellation of gluons attached to colourless particles (see also ref. [8]). A consequence is the loss of one power in $\ln Q^2$ at the leading twist level.

The second example is the projection on the 8_A-state; the projector is $P_{8_A}^{(a_1a_2;a_3a_4)}=\frac{1}{3}f^{a_1a_2c}f^{ca_3a_4}$ which, in addition, has to be normalized by the squareroot of its dimension, since contracting two of these unnormalized projectors is identical to their dimension. (Contraction here means to sum over all indices; it is not only the usual product of projectors.) In the case of colour singlet, with the dimension one, a normalization was unnecessary. Any combination of terms which is symmetric in the indices (12) or (34) cancels out. There is only one term of (2.9) left over:

$$
D_{(4;0)}^{(8_A;-,-)}(k_1,k_2,k_3,k_4) = -g^2\,\frac{3}{4}\,D_{(2;0)}(k_1+k_2,k_3+k_4) \qquad (2.12)
$$

In the 8_A colour state only the term with the correct statistic (odd in both subsytems) survives.

With the help of expression (2.11) we can write down the M^2-integrated version of the cross-section (2.8):

$$
\begin{aligned}
&\frac{d\sigma^{DD}}{dt}(\gamma^*+q\to q\bar{q}+q)\Big|_{t=0} \qquad (2.13)\\
&=\sum_f e_f^2\frac{\alpha_{em}}{8\pi Q^4}\,4\,(2\pi)^3\int\frac{d^2l}{(2\pi)^3}\,\frac{\sqrt{2}}{3}\,\frac{g^2}{l^4}\int\frac{d^2m}{(2\pi)^3}\,\frac{\sqrt{2}}{3}\,\frac{g^2}{m^4}\,D_{(4;0)}^{(1;+,+)}(l,-l,m,-m)
\end{aligned}
$$

A factor $1/8$ stems from the projector P_1 which has to be applied to the lower part in the same way as it was applied before to the fermion loop. It is split up into two factors $1/\sqrt{8}$ for each subsystem (12) and (34). Since the arguments of $D_{(4;0)}$ are normalized by Q, it is convenient to normalize l and m as well. Consequently a $1/Q^4$ arises in front of the expression (2.13) in aggreement with the dimension of the diffractive cross-section at fixed t.

[4] Because of a slightly different color convention, our functions $D_4^{(C,++)}$ ($C=1,8_A,8_S,10+\bar{10}$) differ from those of [9] by an overall minus sign.

For completeness we also include a brief discussion of the (simpler) case of the three-gluon amplitude. It can be thought of as arising from the interference between the production processes of Figs.2.3 and 2.4. The procedure is similar to that of the four-gluon amplitude. The originally eight diagrams can be reduced to three pairs of twisted and non-twisted boxes, and since the whole amplitude is colourless, one pair of gluons is always forced to carry the quantum numbers of the third gluon. In other words one pair of gluons always reggeizes (8_A-reggeon). The overall colour tensor is simply $if^{a_1a_2a_3}$. The analytical expression for the forward direction ($k_1+k_2+k_3=0$) reads:

$$D^{a_1a_2a_3}_{(3;0)}(k_1,k_2,k_3) = g\,i\,f^{a_1a_2a_3}\cdot \left\{D_{(2;0)}(k_1+k_2,k_3) - D_{(2;0)}(k_1+k_3,k_2) + D_{(2;0)}(k_1,k_2+k_3)\right\}\ . \tag{2.14}$$

As it can be seen from (2.9) and (2.11), the function $D_{(2;0)}$ (2.4) plays a rather fundamental role. It therefore seems worthwhile to discuss this function in more detail. For a twist expansion it is convenient to take the Mellin transform with respect to the variable l^2:

$$D_{(2;0)}(l^2) = \int \frac{d\nu}{2\pi i}\,(l^2)^{-\nu}\,\tilde{D}_{(2;0)}(\nu) \tag{2.15}$$

The ν -integration runs along the imaginary axis within the real interval (-1,0). Starting from the second line of (2.4), we rescale l^2 by $\frac{y(1-y)}{\alpha(1-\alpha)}$ and thus get the following result for $\tilde{D}_{(2;0)}$:

$$\begin{aligned}
\tilde{D}_{(2;0)}(\nu) &= \int_0^\infty dl^2\,(l^2)^{\nu-1}\,D_{(2;0)}(l^2)\\
&= \sum_f \frac{e_f^2\alpha_s}{4\pi}\frac{\sqrt{8}}{2\pi}\int_0^1 d\alpha\int_0^1 dy\,4\,\frac{\alpha^{\nu+2}(1-\alpha)^\nu}{y^{\nu-1}(1-y)^{\nu+1}}\int_0^\infty d\bar{l}\,\frac{\bar{l}^\nu}{\bar{l}+1}\\
&= \sum_f \frac{e_f^2\alpha_s}{4\pi}\frac{\sqrt{8}}{2\pi}\,4\,B(\nu+3,\nu+1)\,B(-\nu+2,-\nu)\,B(\nu+1,-\nu)\\
&= \sum_f \frac{e_f^2\alpha_s}{4\pi}\frac{\sqrt{8}}{2\pi}\,\frac{\pi}{4}\,\frac{\Gamma(\nu+3)}{\Gamma(\nu+5/2)}\,\frac{\Gamma(\nu+1)}{\nu+1}\,\frac{\Gamma(-\nu)}{-\nu}\,\frac{\Gamma(-\nu+2)}{\Gamma(-\nu+3/2)}\ .
\end{aligned} \tag{2.16}$$

Since the Γ-functions have poles at negative integer values of their arguments, and we see that $\tilde{D}_{(2;0)}(\nu)$ has a double pole at each integer value of ν except at $\nu=-2$ and $\nu=1$ where it has only simple poles. As usual, a simple pole in the Mellin transform at integer ν leads to a power in l^2 whereas a double pole leads to an additional logarithm. The small-l^2 behavior (which corresponds to the short-distance limit) is obtained if in (2.15) we close the ν-contour to the left and collect the poles at negative integer values. The result is a power expansion with single logarithms which can be interpreted as a twist-expansion. Alternatively, we could close the ν-contour on the right half plane and thus find the large-l^2 behavior of $D_{(2;0)}$. For the coefficients of these expansions one finds:

$$\tilde{D}_{(2;0)} = \sum_f \frac{e_f^2\alpha_s}{4\pi}\frac{\sqrt{8}}{2\pi}\sum_{n=-\infty}^{\infty}\left(\frac{a_n}{\nu+n}+\frac{b_n}{(\nu+n)^2}\right)$$

$$\begin{aligned}
a_1 &= \frac{14}{9}\quad,\quad b_1=\frac{4}{3}\quad;\quad a_2=\frac{2}{5}\quad,\quad b_2=0\\
\text{for } n>2\ :&\\
b_n &= 2(-1)^{n-1}\frac{(n+1)(n-2)}{(2n-3)(2n-1)(2n+1)}\\
a_n &= \left(-\frac{1}{n+1}-\frac{1}{n-2}+\frac{1}{n+1/2}+\frac{1}{n-1/2}+\frac{1}{n-3/2}\right)b_n
\end{aligned} \tag{2.17}$$

As an example, the first three terms of the short-distance expansion are:

$$\begin{aligned}
D_{(2;0)}(l^2) \simeq \sum_f \frac{e_f^2\alpha_s}{4\pi}\frac{\sqrt{8}}{2\pi}\Big\{&\left[\frac{14}{9}-\frac{4}{3}\ln(l^2)\right]l^2+\frac{2}{5}(l^2)^2\\
&+\left[\frac{86}{11025}-\frac{8}{105}\ln(l^2)\right](l^2)^3+\ldots\Big\}
\end{aligned} \tag{2.18}$$

In the leading $\log(Q^2)$ approximation at the leading-twist level only the term $4/3\,\ln(Q^2)\,l^2$ contributes, and it is easy to check that the coefficient $4/3$ is precisely the value of the integrated GLAP- splitting function for a $g\to q\bar{q}$.

This completes our discussion of the fermion loop.

3 Order-α_s Corrections

In this section we go one step beyond the zero order fermion loop calculation and take into account corrections of the order α_s. We now return to the triple-Regge limit and, as before, we shall work in the leading $\log(s)$ approximation. In this limit the smallness of α_s is compensated by a large logarithm in s. Furthermore, corrections inside the fermion loop do not contribute since they do not contribute to the leading power in M^2. We are therefore left only with gluonic corrections below the fermion loop.

As in the previous section we first recapitulate the simpler case of the two-gluon amplitude. The first correction beyond the zero order fermion loop includes the emission of one real gluon. In the Regge limit this gluon is rather soft compared to the incoming particles, the photon and the quark, but not infrared, since the invariant mass of the final state (quark-antiquark-gluon) is assumed to be large. It may be collinear with one of the incoming particles which leads to a divergence as will be seen later. A certain number of diagrams may be neglected using an appropriate gauge. In our case it will be convenient to use the physical lightcone gauge with the gauge condition $p\cdot A=0$ (A denotes the gluon vector potential). This gauge condition suppresses the soft radiation with respect to the quark momentum, since these quasi-Bremsstrahl-gluons are polarized along p. The polarization tensor of the gluon-propagator $d^{\nu\mu}$ and the polarization vectors for the real gluon ϵ^μ have the following form:

$$d^{\nu\mu}(k) = g^{\nu\mu}-\frac{k^\nu p^\mu+p^\nu k^\mu}{k\cdot p} \tag{3.1}$$

$$\epsilon^\mu(k) \;=\; \epsilon_t^\nu(k) - p^\mu \frac{k_t\cdot\epsilon_t(k)}{k\cdot p}\;.$$

(k denotes the gluon momentum). The transverse part of the polarization vector has the following normalization:

$$\begin{aligned}\epsilon_t(k)\cdot\epsilon_t(k) &= -1 \\ \sum \epsilon_t^\nu(k)\epsilon_t^\mu(k) &= -g_t^{\nu\mu}\end{aligned} \tag{3.2}$$

where the sum runs over the two possible orthogonal polarizations in the transverse plane. The Regge kinematics allow to neglect certain pieces of the polarization tensor for t-channel gluons ($k^2 \simeq k_t^2$):

$$\begin{aligned}d^{\nu\mu}(k) &= g_t^{\nu\mu} - 2\,\frac{k_t^\nu p^\mu + p^\nu k_t^\mu + 2\beta_k p^\nu p^\mu}{\alpha_k s} \\ &\simeq -2\,\frac{p^\nu k_t^\mu}{\alpha_k s}\end{aligned} \tag{3.3}$$

where p^ν has to be contracted on the photon side and k_t^μ on quark side.

The complete set of diagrams is shown in Fig. 3.1. The last two diagrams are suppressed, since they contain an extra quark line of large virtuality which is a consequence of requiring a large invariant mass. An important property of the gauge chosen here is the helicity conservation of gluons with a large component in the photon direction [5] (see first diagram of Fig.3.1):

$$\begin{aligned}&\frac{d^{\rho\mu}(k)}{k^2} p^\nu \epsilon^\sigma(k-l)\;\{g_{\mu\nu}(-l-k)_\sigma + g_{\nu\sigma}(2l-k)_\mu + g_{\sigma\nu}(2k-l)_\nu\} \\ =\;& \frac{d^{\rho\mu}(k)}{k^2}\epsilon_\mu(k-l)\,\alpha_k s \;=\; -2\,p^\rho\,\frac{k_t\cdot\epsilon_t(k-l)}{k_t^2}\;.\end{aligned} \tag{3.4}$$

The second diagram of Fig.3.1 gives the following contribution:

$$\begin{aligned}&\bar u(k'-k)\,\hat\epsilon(k-l)\,\frac{(\hat k'-\hat l)}{(k'-l)^2}\,\hat p\,\frac{\hat k'}{k'^2}\,\gamma_t^\mu\,v(q-k') \\ \simeq\;& \bar u(k'-k)\,\hat p\,\frac{(\hat k'-\hat l)}{-2l\cdot k'}\,\hat p\,\frac{\hat k'}{k'^2}\,\gamma_t^\mu\,v(q-k')\,(-2)\,\frac{(k-l)_t\cdot\epsilon_t(k-l)}{\alpha_k s} \\ \simeq\;& \bar u(k'-k)\,\hat p\,\frac{\hat k'}{k'^2}\,\gamma_t^\mu\,v(q-k')\,2\,\frac{(k-l)_t\cdot\epsilon_t(k-l)}{\beta_l\alpha_k s} \\ \simeq\;& \bar u(k'-k)\,\hat p\,\frac{\hat k'}{k'^2}\,\gamma_t^\mu\,v(q-k')\,2\frac{(k-l)_t\cdot\epsilon_t(k-l)}{(k-l)_t^2}\;.\end{aligned} \tag{3.5}$$

In the last line of this equation we have made use of the mass-shell condition $(k-l)^2 = 0$. The third diagram of Fig.3.1 gives the same expression as (3.5), but with opposite sign. The

[5] The same is true for quarks.

commutator relation for the colour tensors allows us to combine eqs.(3.4) and (3.5) which leads to the final result:

$$(-2)\,\left\{\frac{k_t\cdot\epsilon_t(k-l)}{k_t^2} - \frac{(k-l)_t\cdot\epsilon_t(k-l)}{(k-l)_t^2}\right\}\;. \tag{3.6}$$

This expression is well known as the "Lipatov" vertex and can be deduced from [15] by multiplying the expression for the gauge invariant production vertex by $\epsilon^\mu(k-l)$. The use of this "effective" production vertex reduces the number of the eight diagrams of Fig.3.1 to two (Fig.3.2). The singularity at $k_t = l_t$ coming from the second term in (3.6) corresponds to the situation where the emitted gluon is collinear with the upper or lower quark. In the (color zero) Lipatov ladder this singularity is cancelled by the virtual contribution, the divergent piece $\beta(l^2)$ of the gluon Regge-trajectory function $\alpha(l^2)$:

$$\begin{aligned}\alpha(l^2) &= 1+\beta(l^2) \\ \beta(l^2) &= \frac{Ng^2}{2}\int\frac{d^2k}{(2\pi)^3}\frac{l^2}{k^2(k-l)^2} \\ &= Ng^2\int\frac{d^2k}{(2\pi)^3}\frac{l^2}{k^2+(k-l)^2}\frac{1}{(k-l)^2}\end{aligned} \tag{3.7}$$

We now move on to the order-α_s corrections to the diffractive dissociation. The procedure is similar to that used in the previous section. However, we now take the triple Regge limit ($M^2 \gg Q^2$), i.e. we neglect non-logarithmic contributions in the integration over M^2. We add a second t-channel gluon which has to be attached to the diagrams of Fig.3.1 in all possible ways. This produces all the diagrams with the $q\bar q g$ final state. In addition to this, we have the order-α_s correction to the $q\bar q$ final state (Fig.3.8). We then end up with a large number of diagrams which will not be presented here. Instead, we only discuss a few special cases which illustrate general features and then switch to the use of dispersion relations.

Let us begin with the leading $\log(s/M^2)$ contribution (we keep M^2 fixed). As in eq. (2.7) the logarithm follows from the integration over β_{k_1}. In analogy to the case of Fig.2.3 we first mention that as soon as the two t-channel gluons couple to two different lines (quark or gluon) each extra propagator in the loop gives rise to an extra power of $1/\beta_{k_1}$ which suppresses the formation of a logarithm. The same happens when both t-channel gluons are attached to the same line, but the real gluon is emitted in between them. Excluding those non-leading diagrams one is left with the diagrams of Fig.3.3. Beside the planar diagrams one has to add their twisted counterparts (t-channel gluons crossed over) as well, which are not shown explicitly. Just as in eq. (2.7), the leading-$\log(s/M^2)$ result belongs to the colour octet state with odd signature, and each pair of t-channel gluons reggeizes. The reggeized gluons of Fig.3.3 then form the same set of diagrams as in Fig.3.1 which means that the Lipatov vertex is preserved and that the colour octet reggeon behaves exactly like a gluon.

Considering next the imaginary part of the diagrams, it is most instructive to see how the various contributions to the discontinuity in s_1 have to be arranged in order to get the final

result. As illustrated in Fig.3.4, some of the diagrams can be cut in two different ways because they have two s-channel propagators in the upper part of the loop. These two contributions cancel against each other, it seems as if the diagrams would not contribute. The reason for this lies in the appearance of two poles, induced by the two s-channel propagators, in one half of the imaginary β_{k_1}-plane. These two are the only poles. However, it turns out to be more economic to retain these two cut-contributions as two parts of two different effective production vertices (one example is given in Fig.3.5). The use of these Lipatov vertices enables us to reduce the final number of diagrams to ten (Fig.3.6). The final step then consists of taking the square of these diagrams.

At this stage it seems quite clear that it would have been more economic if we would have started from the triple energy discontinuity and, in the unitarity integrals, inserted production amplitudes with the effective gluon production vertex. This would have lead us directly to the square of all diagrams of Fig.3.6. Moreover, the reggeization in the color octet t-channel is obtained automatically from the signature factor in (2.1).

So far we have considered diagrams of diffractive dissociation including only real gluon emission. The virtual contributions to the $q\bar{q}$-system are shown in Fig.3.7. Among others, it includes contributions corresponding to the Regge-trajectory function of the gluons which are necessary to cancel the singularities coming from the BFKL kernel in the first diagram of Fig.3.7. In the leading $\log(s/M^2)$ approximation, where the two gluons reggeize into the colour octet state, the first three contributions of Fig.3.7 combine into one Regge-trajectory function. This result is consistent with the discussion above, since there, we have proven that, in the color octet state all the diagrams can be organized in such a way that the Lipatov production vertex is obtained. In order to end up with a finite cross section we need to add virtual corrections (Fig.3.7) which cancel the collinear divergence. In the case of the colour singlet t-channel state, on the other hand, each set of diagrams in Figs.3.6 or 3.7 is infrared finite by itself.

Before we present a formula for the differential cross section it is convenient to first consider the M^2-integrated case and to combine the diagrams of Figs.3.6 and 3.7. The result is illustrated in Fig.3.8, and it is instructive to analyse these diagrams from the t-channel point of view. There are t-channel intermediate states with two, three and four gluons, and transitions between these states originate from products of effective production vertices. They have been obtained first in [16], and for completeness we present their expressions (see Fig.3.9) [6]:

$$
\begin{aligned}
K_{(2\to 2)} &= -2\,g^2\, f^{b_1 a_1 c} f^{c a_2 b_2}\; q_{1t}^2 q_{2t}^2 \left\{\frac{q_{1t}}{q_{1t}^2} - \frac{(q_1-k_1)_t}{(q_1-k_1)_t^2}\right\}\cdot\left\{\frac{q_{2t}}{q_{2t}^2} - \frac{(q_2-k_2)_t}{(q_2-k_2)_t^2}\right\} \\
&= -g^2\, f^{b_1 a_1 c} f^{c a_2 b_2}\;\cdot \\
&\quad \left\{(k_1+k_2)^2 \;-\; \frac{q_2^2\, k_1^2}{(k_2-q_2)^2} \;-\; \frac{q_1^2\, k_2^2}{(k_1-q_1)^2}\right\}
\end{aligned}
\tag{3.8}
$$

[6] Each letter with the subscript t denotes a 4-vector, i.e. $q_t^2 = -q^2$

$$
\begin{aligned}
K_{(2\to 3)} &= 2\,g^3\, i\, f^{b_1 a_1 c} f^{c a_2 d} f^{d a_3 b_2}\; q_{1t}^2 q_{2t}^2 \left\{\frac{q_{1t}}{q_{1t}^2} - \frac{(q_1-k_1)_t}{(q_1-k_1)_t^2}\right\}\cdot\left\{\frac{q_{2t}}{q_{2t}^2} - \frac{(q_2-k_3)_t}{(q_2-k_3)_t^2}\right\} \\
&= g^3\, i\, f^{b_1 a_1 c} f^{c a_2 d} f^{d a_3 b_2}\;\cdot \\
&\quad \left\{(k_1+k_2+k_3)^2 \;-\; \frac{q_2^2\,(k_1+k_2)^2}{(k_3-q_2)^2} \;-\; \frac{q_1^2\,(k_2+k_3)^2}{(k_1-q_1)^2} \;+\; \frac{q_1^2\, q_2^2\, k_2^2}{(k_1-q_1)^2\,(k_3-q_2)^2}\right\} \\
K_{(2\to 4)} &= -2\,g^4\, f^{b_1 a_1 c} f^{c a_2 d} f^{d a_3 e} f^{e a_4 b_2}\; q_{1t}^2 q_{2t}^2 \left\{\frac{q_{1t}}{q_{1t}^2} - \frac{(q_1-k_1)_t}{(q_1-k_1)_t^2}\right\}\cdot\left\{\frac{q_{2t}}{q_{2t}^2} - \frac{(q_2-k_4)_t}{(q_2-k_4)_t^2}\right\} \\
&= -g^4\, f^{b_1 a_1 c} f^{c a_2 d} f^{d a_3 e} f^{e a_4 b_2}\;\cdot \\
&\quad \left\{-\frac{q_2^2\,(k_1+k_2+k_3)^2}{(k_4-q_2)^2} \;-\; \frac{q_1^2\,(k_2+k_3+k_4)^2}{(k_1-q_1)^2} \;+\; \frac{q_1^2\, q_2^2\,(k_2+k_3)^2}{(k_1-q_1)^2\,(k_4-q_2)^2}\right\}
\end{aligned}
$$

The kernels above already contain a factor $1/2$ due to the Sudakov decomposition. Whereas the first one, the BFKL-kernel, has a singularity at $k_1 = q_1$ which has to be cancelled by the gluon trajectory function, the other two do not have such a singularity.

Before we actually can sum up our analytical expressions we remark on the colour structure. Again, as in the subsection before, we find it most convenient to write all tensors in terms of those "basis" tensors which we have introduced before for the fermion loop. It turns out that the order-α_s diagrams have a color structure which is rather similar to that of the fermion loop. It is therefore straightforward to express the final result in terms of these simple colour tensors. One examples are given in Fig.3.10.

With this information we now turn to the main result of this section, namely the sum of all diagrams (Fig.3.8). It is useful to remember that the fermion loop with three and four gluons can be expressed in terms of $D_{(2;0)}$ (see eqs.(2.14) and (2.9)). This allows to rewrite the diagrams of Fig.3.8 in the form illustrated in the second line of Fig.3.8: two reggeized gluons couple to the fermion loop, and, somewhere between the quark loop at the top and the four-gluon state at the bottom of the diagram, we have a transition from two to four gluon lines. Using this way of presenting the sum of all diagrams, we parametrize the transverse momentum loop integral in such a way that the momentum of the gluon in the two-gluon intermediate state is denoted by k. After these preparatory remarks it is not difficult to understand which form the sum of all diagrams will have. First, we expect that the reggeization found in the previous section continues to all orders in α_s. The most obvious example is the color octet channel of the (12) and (34) subsystems: here one expects to see $D_2(k_1+k_2, k_3+k_4)$. Similar considerations (although, maybe, less obvious) apply to the remaining terms in (2.9). Once these "reggeization" pieces have been separated out, the remaining terms should be organized as sums of diagrams with two or four reggeizing gluons in the t-channel. The transition from the two-gluon state to the four-gluon state is mediated by an effective transition vertex, consisting of both connected and disconnected pieces, and the form of this vertex should follow from our order-α_s corrections. This general form of the final result has been discussed already in [9].

The main observation now and one of the key results of this paper is the fact that both the effective transition vertex and the BFKL-kernel can be expressed in terms of a single

function G. As it was said before, the effective transition vertex can be read off from the sum of all our diagrams, if we subtract the α_s corrections to the reggeization terms in (2.9). We therefore write for the sum of all diagrams:

$$
\begin{aligned}
&D^{a_1a_2a_3a_4}_{(4;1)}(x,k_1,k_2,k_3,k_4) \;=\; \frac{g^2}{2\sqrt{2}}\;\cdot \\
&\Big\{\, d^{a_1a_2a_3a_4}\, D_{(2;1)}(x,k_1,k_2+k_3+k_4) \;+\; d^{a_2a_1a_3a_4}\, D_{(2;1)}(x,k_2,k_1+k_3+k_4) \\
&+ d^{a_3a_2a_4a_1}\, D_{(2;1)}(x,k_3,k_1+k_2+k_4) \;+\; d^{a_4a_2a_3a_1}\, D_{(2;1)}(x,k_4,k_1+k_2+k_3) \qquad (3.9)\\
&-\frac{1}{4} f^{a_1a_2c} f^{ca_3a_4}\, D_{(2;1)}(x,k_1+k_2,k_3+k_4) - \frac{1}{4} f^{a_1a_3c} f^{ca_2a_4}\, D_{(2;1)}(x,k_1+k_3,k_2+k_4) \\
&-\frac{1}{4} f^{a_1a_4c} f^{ca_2a_3}\, D_{(2;1)}(x,k_1+k_4,k_2+k_3) \\
&-\frac{1}{4} d^{a_1a_2c} d^{ca_3a_4}\, D_{(2;1)}(x,k_1+k_2,k_3+k_4) - \frac{1}{4} d^{a_1a_3c} d^{ca_2a_4}\, D_{(2;1)}(x,k_1+k_3,k_2+k_4) \\
&-\frac{1}{4} d^{a_1a_4c} d^{ca_2a_3}\, D_{(2;1)}(x,k_1+k_4,k_2+k_3) \\
&-\frac{1}{6} \delta^{a_1a_2} \delta^{a_3a_4}\, D_{(2;1)}(x,k_1+k_2,k_3+k_4) - \frac{1}{6} \delta^{a_1a_3} \delta^{a_2a_4}\, D_{(2;1)}(x,k_1+k_3,k_2+k_4) \\
&-\frac{1}{6} \delta^{a_1a_4} \delta^{a_2a_3}\, D_{(2;1)}(x,k_1+k_4,k_2+k_3) \Big\} \\
&+ \ln(1/x)\; D_{(2;0)} \otimes V^{a_1a_2a_3a_4}(x,k_1,k_2,k_3,k_4)\;\;.
\end{aligned}
$$

Here $D_{(2;1)}$ describes the usual BFKL-ladder consisting of the fermion loop and order α_s corrections:

$$
\begin{aligned}
D_{(2;1)}(x,a,-a) \;&=\; \ln(1/x) \int \frac{d^2k}{(2\pi)^3}\, \frac{1}{k^4}\; D_{(2;0)}(k^2)\; K_{2\to 2}(k^2;a,-a) \\
&=\; \ln(1/x)\; D_{(2;0)} \otimes K_{2\to 2}(a,-a)\;\;. \qquad (3.10)
\end{aligned}
$$

The term in the last line describes the transition vertex two reggeon $\to$ four gluon. The logarithm in $1/x$ results from the logarithmic integration over M^2. The transition vertex V finally consists of a sum of several terms:

$$
\begin{aligned}
&V^{a_1a_2a_3a_4}(k_1,k_2,k_3,k_4) \;=\; \frac{g^2}{12\sqrt{2}}\;\cdot \qquad (3.11)\\
&\{\, \delta^{a_1a_2}\delta^{a_3a_4}\; [\,G(k_1,k_3)+G(k_2,k_3)+G(k_1,k_4)+G(k_2,k_4) \\
&\qquad -G(k_1,k_3+k_4)-G(k_2,k_3+k_4)-G(k_3,k_1+k_2)-G(k_4,k_1+k_2) \\
&\qquad +G(k_1+k_2,k_3+k_4)\,] \\
&+\,\delta^{a_1a_3}\delta^{a_2a_4}\; [\,G(k_1,k_2)+G(k_3,k_4)+G(k_2,k_3)+G(k_1,k_4) \\
&\qquad -G(k_1,k_2+k_4)-G(k_2,k_1+k_3)-G(k_3,k_2+k_4)-G(k_4,k_1+k_3) \\
&\qquad +G(k_1+k_3,k_2+k_4)\,] \\
&+\,\delta^{a_1a_4}\delta^{a_1a_3}\; [\,G(k_1,k_2)+G(k_3,k_4)+G(k_1,k_3)+G(k_2,k_4)
\end{aligned}
$$

$$
\begin{aligned}
&\qquad -G(k_1,k_2+k_3)-G(k_2,k_1+k_4)-G(k_3,k_1+k_4)-G(k_4,k_2+k_3) \\
&\qquad +G(k_1+k_4,k_2+k_3)\,]\,\}\;\;.
\end{aligned}
$$

In this sum, the new function G appears which has the following form:

$$
\begin{aligned}
D_{(2;0)} \otimes G(a,b) \;&=\; 3\,g^2 \int \frac{d^2k}{(2\pi)^3}\;\cdot \qquad (3.12)\\
&\Big\{ \Big[\frac{a^2}{(k-a)^2k^2} + \frac{b^2}{(k+b)^2k^2} - \frac{(a+b)^2}{(k-a)^2(k+b)^2} \Big]\; D_{(2;0)}(k^2) \\
&\quad - \frac{1}{(k-a)^2} \Big[\frac{a^2}{(k-a)^2+k^2} - \frac{(a+b)^2}{(k-a)^2+(k+b)^2} \Big]\; D_{(2;0)}(a^2) \\
&\quad - \frac{1}{(k+b)^2} \Big[\frac{b^2}{(k+b)^2+k^2} - \frac{(a+b)^2}{(k+b)^2+(k-a)^2} \Big]\; D_{(2;0)}(b^2) \Big\}\;\;.
\end{aligned}
$$

In the forward direction, i.e $a+b$ equal zero, G is identical to the usual Lipatov kernel including the trajectory functions. For a or b equal zero G becomes zero. There are no infrared divergencies.

Before we study this new function G in more detail, a few words should be said about the transition vertex V. It has some nice properties. First of all, it is completely symmetric under the interchange of the external legs, i.e. under simultanous interchange of the momenta k_i and the colour indices a_i. Later on we shall show that this symmetry plays a very important role in proving the AGK-cutting rules. Secondly, V goes to zero whenever one of the k_i does. This property becomes relevant when we perform a twist analysis (see [9]). Finally, the simplicity of V looks very appealing: it has a simple colour structure, and we need only one function G in order to describe the dependence on the momenta k_i.

The form (3.11) of the effective transition vertex is not unique. In particular, in (3.9) the terms proportional to $\delta^{a_ja_k}\delta^{a_la_m}$ have the same color structure as V in (3.11), and it is therefore possible to absorb them into the definition of a modified transition vertex $\tilde{V}$. From the point of view of Regge-physics one would even prefer this version since in (3.9) these terms seem to suggest that there is a color singlet reggeon in the theory which is not the case. On the other hand, the new vertex $\tilde{V}$ does not have the same nice properties which V has, in particular it does not vanish when one of the k_i goes to zero. This feature becomes important when a twist-analysis is performed, and we therefore conclude that the form (3.11) is what we should use in short-distance dominated reactions. For the rest of this paper we shall stick to (3.11), but we keep in mind that this form is not unique.

We now return to our original goal of this section, namely the lowest order cross section for the diffractive dissociation $\gamma^* + q \to q\bar{q}g + q$. This cross section can also be expressed in terms of our function G. We go back to Fig.3.6, square the diagrams and project on colour singlet in the subsystems (12) and (34). We arrive at a set of diagrams similar to that in Fig.3.8, but without the virtual contributions of Fig.3.7. For the sum of these diagrams we obtain an expression which again uses the G-function. Overall constants are obtained as in

(2.13); in addition the factor $1/M^2$ appears, reflecting the fact that we are working in the triple Regge limit:

$$\frac{d\sigma^{DD}}{dt\,dM^2}(\gamma^* + q \to q\bar{q}g + q)\Big|_{t=0} = \sum_f e_f^2 \frac{\alpha_{em}}{8\pi Q^4} \frac{4(2\pi)^3}{M^2} \int \frac{d^2l}{(2\pi)^3} \frac{\sqrt{2}}{3} \frac{g^2}{l^4} \int \frac{d^2m}{(2\pi)^3} \frac{\sqrt{2}}{3} \frac{g^2}{m^4} \cdot$$
$$\cdot \frac{3\,g^2}{4\sqrt{2}} D_{(2;0)} \otimes \{\, 2G(l,-l) + 2G(m,-m) + 2G(l,m) + 2G(l,-m)$$
$$+ G(l+m,-l-m) + G(l-m,m-l) \qquad (3.13)$$
$$- 2G(l,m-l) - 2G(-l,l+m) - 2G(m,l-m) - 2G(-m,l+m) \,\} \;.$$

We have put $k_1 = -k_2 = l$ and $k_3 = -k_4 = m$ and normalized l and m by Q.

In the remainder of this section we study the function G in somewhat more detail. Starting from (3.12) we recognize that the integration over the azimuth angle of k can be evaluated explicitly:

$$D_{(2;0)} \otimes G(a,b) = \frac{3\,g^2}{(2\pi)^2} \cdot \qquad (3.14)$$
$$\left\{ \int_0^\infty \frac{dk^2}{k^2} \frac{k^2\,a\cdot b + a^2\,b^2}{k^4 + 2k^2\,a\cdot b + a^2\,b^2} \left[\Theta(k^2-a^2) - \Theta(b^2-k^2)\right] D_{(2;0)}(k^2) \right.$$
$$\left. - \ln\left(\frac{|a|}{|a+b|}\right) D_{(2;0)}(a^2) - \ln\left(\frac{|b|}{|a+b|}\right) D_{(2;0)}(b^2) \right\} \;.$$

As it was noticed already in the previous subsection it is very convenient to use the Mellin transformation, especially in order to discuss the twist expansion. Substituting into (3.14) for $D_{(2;0)}$ its Mellin transform (2.16) and performing the integration over k^2, we arrive at a new representation of G:

$$D_{(2;0)} \otimes G(a,b) = \int \frac{d\nu}{2\pi i}\, \tilde{D}_{(2;0)}(\nu)\, \tilde{G}(\nu,a,b) \qquad (3.15)$$

with

$$\tilde{G}(\nu,a,b) = \frac{3\,g^2}{(2\pi)^2} \left\{ \int_0^\infty \frac{dk^2}{k^2} \frac{k^2\,a\cdot b + a^2\,b^2}{k^4 + 2k^2\,a\cdot b + a^2\,b^2} \left[\Theta(k^2-a^2) - \Theta(b^2-k^2)\right] (k^2)^{-\nu} \right.$$
$$\left. - \ln\left(\frac{|a|}{|a+b|}\right) (a^2)^{-\nu} - \ln\left(\frac{|b|}{|a+b|}\right) (b^2)^{-\nu} \right\} \;. \qquad (3.16)$$

The k^2-integration can be done explicitly, using complex variables

$$2\,a\cdot b = |a|\,|b|\left(e^{i\theta} + e^{-i\theta}\right) \qquad (3.17)$$

and the following factorization of the denominator in (3.16):

$$k^4 + 2k^2\,a\cdot b + a^2\,b^2 = \left(k^2 + |a|\,e^{i\theta}\right)\left(k^2 + |b|\,e^{-i\theta}\right) \;. \qquad (3.18)$$

(θ denotes the angle between a and b). We finally end up with:

$$\tilde{G}(\nu,a,b) = \frac{3\,g^2}{(2\pi)^2}\,\Theta(|a|-|b|) \left\{ \left(\ln\left(\frac{|a|}{|b|}\right) - \frac{1}{\nu}\right)(b^2)^{-\nu} \right. \qquad (3.19)$$
$$\left. + \sum_{n=1}^{\infty} \left(-\frac{|b|}{|a|}\right)^n \cos(n\theta) \left[\left(\frac{1}{n+\nu} - \frac{1}{n}\right)(a^2)^{-\nu} + \left(\frac{1}{n-\nu} - \frac{1}{n}\right)(b^2)^{-\nu} \right] \right\}$$
$$+ \;(|a| \leftrightarrow |b|) \;.$$

Taking the forward direction $a+b=0$ we obtain the well-known form of the Lipatov kernel in the ν-representation:

$$\tilde{G}(\nu,a,-a) = \frac{3\,g^2}{(2\pi)^2} \left\{2\psi(1) - \psi(-\nu) - \psi(1+\nu)\right\} (a^2)^{-\nu} \qquad (3.20)$$
$$\psi(\nu) = \frac{d\ln\Gamma(\nu)}{d\nu} \;.$$

It should be remarked that the Mellin transformation of D_2 was originally defined for ν lying in the interval (-1,0). Having found analytic expressions $\tilde{D}_{(2;0)}$ and $\tilde{G}$ we can analytically continue our Mellin transform into the whole complex ν-plane, where $\tilde{D}_{(2;0)}$ and $\tilde{G}$ are well defined. Depending on the values of $|a|$ or $|b|$, we can close the contour of the ν integration either to the right or to the left of the imaginary axis. As in the case of D_2, the latter case corresponds to the twist expansion. The leading pole of $\tilde{G}$ is located at $\nu = -1$. A second point which we would like to mention is the fact that the logarithm $\ln|a+b|$ in (3.16) is responsible for the subtraction $1/n$ in eq.(3.19). It ensures that the sum over n converges even for $\theta = \pi$. This reflects the cancellation of infrared divergencies between the connected and disconnected diagrams. Finally, we would like to remark that $\tilde{G}$ becomes zero as soon as one of the two arguments $|a|$ or $|b|$ vanishes. In this case we have to restrict the ν -values to the left of the imaginary axis.

4 All Orders: the Triple Pomeron Vertex

In this section we shall first show that the structure of the transition vertex which we have obtained in the previous section remains valid in all orders of the strong coupling α_s. This result then will enable us to cast the cross section for diffractive dissociation in such a form that the triple Pomeron vertex appears.

For the first part of this section we shall use the same idea as presented in [9]: the sum of all diagrams can be written in terms of an integral equation, and this equation can be rewritten in such a way that the vertex (3.11) emerges. As we have said before, the starting point of our calculation is the triple-energy discontinuity which leads to the partial wave F of (2.1). We make use of the leading-log s production amplitudes $T_{n\to m}$, and all phase-space integrals are done in the multiperipheral approximation where all subenergies s_{ij} are small compared to the total energy s, and all momentum transfers t_i are finite. The result for this

discontinuity is illustrated in Fig.4.1: wavy vertical lines denote (reggeized) gluons with a propagator $1/k^2$, the analytic expressions for the vertices which change the number of gluon lines are given in (3.8), and the interaction between gluon lines is described by the BFKL-kernel (3.8). The first interaction between the two ladders at the bottom will be referred to as the branching vertex. The singularity structure in the three angular momentum variables (in the following we shall use the notation $\omega = j - 1$, $\omega_1 = j_1 - 1$, and $\omega_2 = j_2 - 1$) is obtained from the following rules: for each t-channel intermediate state above the branching vertex there is "reggeon propagator" $1/(\omega - \sum_i(\alpha_i - 1))$ (where α_i stands for the trajectory function $\alpha(k_i^2) = 1 + \beta(k_i^2)$, and the sum extends over the gluon lines with momenta k_i). Analogously, for each intermediate state in the t_1 (t_2) channel we have a reggeon propagator $1/(\omega_1 - \beta_1 - \beta_2)$ ($1/(\omega_2 - \beta_1 - \beta_2)$). Each transverse momentum integral comes with a $\frac{d^2k}{(2\pi)^3}$, and sometimes we shall use the notation $\otimes$ to abbreviate such an integration together with the necessary propagators $1/k^2$ for internal vertical gluon lines (cf.(3.10)). Finally, the expressions for the kernels are given in (3.8), and there is an overall factor of 4 in front of the amplitude. All constants not contained in these rules will be written explicitly.

The sum of the diagrams in Fig.4.1 can conveniently be reorganized by introducing the functions D_2, D_3, and D_4, resp., which depend only on the single angular momentum variable ω and satisfy the integral equations illustrated in Fig.4.2. They are nonamputated, i.e. they include a reggeon propagator for the external gluon lines. The amputated counterparts will be denoted by C_2, C_3, and C_4, resp., and the connection is given by, e.g.,

$$D_2(\omega, k, q-k) = C_2(\omega, k, q-k)\frac{1}{(\omega + 2 - \alpha(k) - \alpha(q-k))}. \tag{4.1}$$

In addition, we introduce a Green's function $G_{2\to 2}(\omega)$ which is illustrated in Fig.4.3 and also is defined to include reggeon propagators for the external gluon lines. All these functions are tensors in color space. Using this notation, Fig.4.1 can be rewritten as illustrated in Fig.4.4. Let us first discuss the part above the branching vertex, i.e. the function D_4 (and C_4). Whereas the lowest order contributions have been discussed in the previous section, the integral equations (Fig.4.2) for the all-order expression have been derived and studied in [9]. Details of this equation will not be needed here and we give only a general description of the arguments. We begin by rearranging the last equation of Fig.4.2. in the following way. We write the amplitude D_4 as a sum of the "reggeizing" terms D_4^R and the remainder D_4^I (" irreducible" with respect to reggeization)[7]:

$$D_4 = D_4^R + D_4^I. \tag{4.2}$$

The reggeization piece D_4^R is the all-order generalization of (2.9): in the ω representation we have

$$D_4^{R\,a_1a_2a_3a_4}(k_1, k_2, k_3, k_4; \omega) \;=\; \frac{g^2}{2\sqrt{2}}\cdot$$

[7] In [9] a slightly different notation was used: $D_{4;2-cut}$ instead of D_4^R, and $D_{(4;R)}$ instead of D_4^I.

$$\begin{aligned}
&\{\, d^{a_1a_2a_3a_4} D_2(k_1, k_2+k_3+k_4;\omega) \;+\; d^{a_2a_1a_3a_4} D_2(k_2, k_1+k_3+k_4;\omega)\\
&+ d^{a_1a_2a_4a_3} D_2(k_3, k_1+k_2+k_4;\omega) \;+\; d^{a_1a_2a_3a_4} D_2(k_4, k_1+k_2+k_3;\omega)\\
&-\frac{1}{4} f^{a_1a_2c} f^{ca_3a_4} D_2(k_1+k_2, k_3+k_4;\omega) - \frac{1}{4} f^{a_1a_3c} f^{ca_2a_4} D_2(k_1+k_3, k_2+k_4;\omega)\\
&-\frac{1}{4} f^{a_1a_4c} f^{ca_2a_3} D_2(k_1+k_4, k_2+k_3;\omega)\\
&-\frac{1}{4} d^{a_1a_2c} d^{ca_3a_4} D_2(k_1+k_2, k_3+k_4;\omega) - \frac{1}{4} d^{a_1a_3c} d^{ca_2a_4} D_2(k_1+k_3, k_2+k_4;\omega)\\
&-\frac{1}{4} d^{a_1a_4c} d^{ca_2a_3} D_2(k_1+k_4, k_2+k_3;\omega)\\
&-\frac{1}{6} \delta^{a_1a_2}\delta^{a_3a_4} D_2(k_1+k_2, k_3+k_4;\omega) - \frac{1}{6} \delta^{a_1a_3}\delta^{a_2a_4} D_2(k_1+k_3, k_2+k_4;\omega)\\
&-\frac{1}{6} \delta^{a_1a_4}\delta^{a_2a_3} D_2(k_1+k_4, k_2+k_3;\omega)\Big\}\;,
\end{aligned} \tag{4.3}$$

and each D_2 satisfies the BFKL equation. We would like to remark that, strictly speaking, the Regge propagator $1/(\omega - \sum\beta_i)$ or the trajectory function $\alpha_i = 1 + \beta_i$ respectively is infrared divergent. Nevertheless, we know that these divergencies are cancelled by similar divergencies of the BFKL-kernels which was proven in the finite order calculation (section 3). The same holds for the all-order generalization. The easiest way to prove this is by multiplying, in Fig.4.2, the last integral equation for D_4 by $\omega - \beta_1 - \beta_2 - \beta_3 - \beta_4$ and combining the trajectory functions with the BFKL-kernels in the last term. This leads to the BFKL-like equation for D_4 given in [9], and there it has been shown that each BFKL-kernel can be combined with trajectory functions in just the right way to cancel the infrared divergencies. Returning now to the decomposition (4.2), we subtract the reggeizing piece D_4^R on both sides of the integral equation for D_4 and obtain a modified equation for the irreducible part D_4^I:

$$\begin{aligned}
\omega\, D_4^I = D_2 \otimes K_{2\to 4} + D_3 \otimes \sum K_{2\to 3} + D_{(4;0)} - \omega D_4^R + D_4^R \otimes \sum(K_{2\to 2} + \alpha - 1)\\
+ D_4^I \otimes \sum(K_{2\to 2} + \alpha - 1).
\end{aligned} \tag{4.4}$$

On the rhs the fourth term is the function D_4^R which consists of a sum of D_2 functions. For each of them we write its BFKL equation and insert it into the eq. (4.4); the inhomogenous terms then cancel against $D_{(4;0)}$. The result is:

$$\begin{aligned}
\omega\, D_4^I = D_2 \otimes K_{2\to 4} + D_3 \otimes \sum K_{2\to 3} - \sum D_2 \otimes K_{2\to 2} + D_4^R \otimes \sum(K_{2\to 2} + \alpha - 1)\\
+ D_4^I \otimes \sum(K_{2\to 2} + \alpha - 1).
\end{aligned} \tag{4.5}$$

All terms in the first line define the inhomogeneous part of the integral equation. As shown in (4.3), D_4^R is expressed as a sum of D_2 functions. For D_3 (its integral equation is illustrated by the second line of Fig.4.2) we know from [9] that it can also be expressed in terms of D_2:

$$\begin{aligned}
D_3^{a_1a_2a_3}(k_1, k_2, k_3;\omega) \;&=\; g\, i\, f^{a_1a_2a_3}\cdot\\
&\{D_2(k_1+k_2, k_3;\omega) - D_2(k_1+k_3, k_2;\omega) + D_2(k_1, k_2+k_3;\omega)\}\;.
\end{aligned} \tag{4.6}$$

Consequently, all pieces of the inhomogeneous term in eq.(4.5) can be written as $D_2 \otimes V$, and V can be shown to coincide with (3.11). Namely, if we compare (4.5) with Fig.3.8 we immediately see the transition vertex has the same form (the only difference between Fig.3.8 and the first line of (4.5) lies in the expression for the part above the transition vertex. In the first case it is $D_{(2,0)}$, whereas in the second case we have the full D_2 function).

Next we rewrite (3.11) in terms of the group decomposition used in [9]. Starting from (3.11) we first notice that there is no odd-signature contribution. Next we project on irreducible representations in the (12) and (34) subsystems, using the projectors given in the appendix of [9]. We obtain:

$$8V(1234) + V(1324) + V(1423) \tag{4.7}$$

$$\sqrt{8}(-V(1324) + V(1423)) \tag{4.8}$$

$$\sqrt{8}(V(1324) + V(1423)) \tag{4.9}$$

$$\sqrt{20}(-V(1324) + V(1423)) \tag{4.10}$$

$$\sqrt{27}(V(1324) + V(1423)) \tag{4.11}$$

for the representations 1, 8_A, 8_S, $10 + \overline{10}$, and 27, resp. (note that we do not consider 10 and $\overline{10}$ seperately). The function $V(1234)$ has the form:

$$\begin{aligned} \frac{g^2}{12\sqrt{2}} \quad & [G(k_1,k_3) + G(k_2,k_3) + G(k_1,k_4) + G(k_2,k_4) \\ & -G(k_1,k_3+k_4) - G(k_2,k_3+k_4) - G(k_3,k_1+k_2) - G(k_4,k_1+k_2) \\ & +G(k_1+k_2,k_3+k_4)]. \end{aligned} \tag{4.12}$$

We finally mention that this result for the transition vertex can be obtained also directly from the integral equation of [9]. Namely, casting eqs.(2.11) of [9] into the form (4.5), we obtain, for the color singlet case, after some lengthy algebra, the combination (4.7). Repeating the same steps for the other representations, one calculates the other combinations in (4.7) - (4.11). Forming appropriate linear combinations, it is then possible to extract the function $V(1234)$ which is found to agree with (4.12) and (3.12).

This completes our proof that the transition vertex which we have found in the previous section remains valid to all orders. Thus we can represent the function D_4 in a rather compact form: following (4.2), it consists of two pieces, the reggeizing part and the irreducible part (Fig.4.5). The latter one is described as follows: starting from above, we first have a two-gluon t-channel state, then a transition to a four-gluon state which is described by our vertex V. In the four-gluon state, we have pairwise interactions given by the BFKL kernel. In an obvious notation we can write:

$$D_4^I = D_2 \otimes V \otimes G_{4\to 4}, \tag{4.13}$$

where the Green's function $G_{4\to 4}$ is the four-gluon Green's function which contains all pairwise gluon interactions.

Now let us return to the triple energy discontinuity shown in Fig.4.1. We first remove the coupling to the quarks at the bottom and are left with a new form of a four-gluon amplitude (Fig.4.4): it depends upon the three angular momentum variables ω, ω_1, and ω_2 (the precise rules have been described at the beginning of this section), and the function is defined to include reggeon denominators at the bottom. As illustrated in the first line of Fig.4.4, we use the functions C_2, C_3, and C_4 to express the diagrams for this amplitude in a rather compact fashion. Next we add and subtract the terms with one interaction between the gluon lines 1,2 and 3, 4: this allows to use the integral equation for C_4 (see Fig.4.2), and we arrive at the second line of Fig.4.4. According to the rules which we have stated above, the function C_4 dependes upon ω and is amputated, i.e. does not include a reggeon propagator for the outgoing gluon lines. In the second and third term, however, a propagator for the interemediate state above the last interaction is included. As an example, for the second term: $1/(\omega - \beta_1' - \beta_2' - \beta_3 - \beta_4)$ where the prime symbols indicate that the arguments of the trajectory functions belong to internal lines. The Green' functions $G_{2\to 2}$ depend upon the angular momenta ω_1 or ω_2, and they are defined to include reggeon propagators at both ends. We rewrite the second line of Fig.4.4 in the following way:

$$\begin{aligned} & \left[C_4 - \frac{C_4 \otimes K_{2\to 2}(12)}{(\omega - \beta_1' - \beta_2' - \beta_3 - \beta_4)} - \frac{C_4 \otimes K_{2\to 2}(34)}{(\omega - \beta_1 - \beta_2 - \beta_3' - \beta_4')}\right] \otimes G^{(0)}_{2\to 2}(\omega_1) G^{(0)}_{2\to 2}(\omega_2) \\ = \; & C_4 \otimes G^{(0)}_{2\to 2}(\omega_1) G^{(0)}_{2\to 2}(\omega_2) - C_4 \frac{\omega_1 - \beta_1' - \beta_2'}{(\omega - \beta_1' - \beta_2' - \beta_3' - \beta_4')} \otimes G^{(1)}_{2\to 2}(\omega_1) G^{(0)}_{2\to 2}(\omega_2) \\ - \; & C_4 \frac{\omega_2 - \beta_3' - \beta_4'}{(\omega - \beta_1' - \beta_2' - \beta_3' - \beta_4')} \otimes G^{(0)}_{2\to 2}(\omega_1) G^{(1)}_{2\to 2}(\omega_2) \end{aligned} \tag{4.14}$$

(for the distinction between $G^{(0)}_{2\to 2}$ and $G^{(1)}_{2\to 2}$ see Fig.4.3). As long as $M^2 \ll s$, (4.14) can be simplified further: in the second term, we write $G^{(1)}_{2\to 2}(\omega_1) = G^{(0)}_{2\to 2}(\omega_1) - 1/[(\omega_1 - \beta_1 - \beta_2) k_1^2 k_2^2]$. When doing the ω_1-integral, the ω_1 singularity in the second term cancels and thus gives zero contribution. The third term in (4.14) is rewritten in an analogous way. Combination of the three terms yields:

$$C_4 \frac{\omega - \omega_1 - \omega_2}{(\omega - \beta_1' - \beta_2' - \beta_3' - \beta_4')} \otimes G^{(0)}_{2\to 2}(\omega_1) G^{(0)}_{2\to 2}(\omega_2). \tag{4.15}$$

If on the other hand we integrate over M^2, it is convenient to cast (4.12) into a slightly different form and to seperate the terms with no interaction in system (12) or (34). We obtain:

$$\begin{aligned} & C_4 \frac{1}{(\omega_1 - \beta_1 - \beta_2)(\omega_2 - \beta_3 - \beta_4)} \\ + \; & C_4 \frac{\omega - \omega_2 - \beta_1 - \beta_2}{(\omega - \beta_1 - \beta_2 - \beta_3' - \beta_4')(\omega_1 - \beta_1 - \beta_2)} \otimes G^{(1)}_{2\to 2}(\omega_2) \\ + \; & C_4 \frac{\omega - \omega_1 - \beta_3 - \beta_4}{(\omega - \beta_1' - \beta_2' - \beta_3 - \beta_4)(\omega_2 - \beta_3 - \beta_4)} \otimes G^{(1)}_{2\to 2}(\omega_1) \\ + \; & C_4 \frac{\omega - \omega_1 - \omega_2}{(\omega - \beta_1' - \beta_2' - \beta_3' - \beta_4')} \otimes G^{(1)}_{2\to 2}(\omega_1) G^{(1)}_{2\to 2}(\omega_2). \end{aligned} \tag{4.16}$$

If we now integrate in (2.2) over M^2, we obtain a pole $1/(\omega-\omega_1-\omega_2)$ which enforces the conservation of angular momenta $\omega_1+\omega_2=\omega$. In the last three terms of (4.16), this pole is cancelled by the ω-numerators: as a result, the contour of one of the ω_i-integrations can be closed to the right hand side and gives zero. The first term, after integration over ω_1, coincides with D_4.

In order to arrive at a formula for the diffractive dissociation cross section (at fixed M^2), we make use of (4.15) (Fig.4.5), decompose C_4 according to (4.2) and, for the rest of this section, restrict ourselves to color singlets in the two lower legs. For the first term, $C_4^R=D_4^R(\omega-\sum_i\beta_i')$, we use the form (4.3). When coupling this part to the Green's functions in the lower legs, the following vertex function V^R appears:

$$\begin{aligned} & V^R(\omega;q_1,-q_1;k_1,k_2,k_3,k_4) \\ = \; & g^2\,\frac{\sqrt{2}}{3}\left[\delta^{(2)}(q_1-k_2-k_3-k_4)+\delta^{(2)}(q_1-k_1-k_3-k_4)\right. \\ & \quad +\delta^{(2)}(q_1-k_1-k_2-k_4)+\delta^{(2)}(q_1-k_1-k_2-k_3) \\ & \quad \left.-\delta^{(2)}(q_1-k_1-k_2)-\delta^{(2)}(q_1-k_1-k_3)-\delta^{(2)}(q_1-k_1-k_4)\right]. \end{aligned} \tag{4.17}$$

As the distinctive feature of this contribution, there is no four-gluon state above this vertex V^R. The second part, containing C_4^I from (4.13), requires no further simplification; we only emphasize that it contains, right above the branching vertex, the four gluon state with all its interactions between the gluon lines.

We are now in the position to write our final formula for the diffractive dissociation cross section. It has the form (2.2), and the partial wave consists of the two pieces:

$$\begin{aligned} F(j,j_1,j_2;0,t,t) \;=\; & 4\;(\omega-\omega_1-\omega_2)\;\cdot \\ & \cdot\left(D_2\otimes V^R+D_2\otimes V\otimes G_{4\to4}\right)\otimes G_{2\to2}^{(0)}(\omega_1)G_{2\to2}^{(0)}(\omega_2) \\ & \otimes\left(\frac{\sqrt{2}g^2}{3}\right)\;\left(\frac{\sqrt{2}g^2}{3}\right). \end{aligned} \tag{4.18}$$

The last line contains the contribution of the coupling of the two lower ladders to the quarks at the bottom. We emphasize that this expression is infrared finite provided we replace the quarks by colorless objects. The proof of this statement is seen most easily from the first line in (4.14): the infrared finiteness of the expression in square brackets follows from [9]. The two functions $G_{2\to2}^{(0)}$, when convoluted with suitable couplings to color singlet particles at the bottom, turn into infrared finite BFKL Pomerons.

From (4.18) we now extract our result for the triple Pomeron vertex (Fig.4.5). Obviously, the two lower ladders stand for BFKL Pomerons; in the upper part of the second term, however, we see, in D_2, the BFKL Pomeron *and*, in $G_{4\to4}$, the four gluon state. This shows that, above the vertex, the Pomeron is not the same as below, but it appears as a superposition of the two and four gluon states; to neglect the latter one would destroy the reggeization properties that have lead to D_4^R and is, therefore, illegitimate. As a result, the

Pomeron exchanged in this quasi-elastic process: *photon + Pomeron → photon + Pomeron* is not the same as in the elastic reaction *photon + photon → photon + photon*. The fact that the (perturbative) Pomeron appears to be dependent upon to what it couples (to a Pomeron through the triple Pomeron coupling (PPP) or to a virtual photon ($\gamma^*P\gamma^*$)) hints at a deeper defect of the BFKL-approximation (and any finite order perturbative unitarity correction to it).

5 The AGK-Cutting Rules

In this section we briefly outline how our perturbative results manage to satisfy the Abramovsky-Gribov-Kanchelli (AGK) cutting rules. In their original form they have been stated for the elastic scattering amplitude. They give a prescription how the imaginary part of a Regge-cut amplitude can be written as a sum of different contributions to the unitarity integral:

$$disc_s T_{2\to2}=\frac{1}{i}\left[T_{2\to2}-T_{2\to2}^*\right]=\sum_n T_{2\to n}T_{2\to n}^*. \tag{5.1}$$

We shall stick to the easiest case and investigate the four reggeon cut contribution to the elastic scattering of two virtual photons which, among other contributions, contains the two-Pomeron cut.

Again it will be instructive to first recapitulate the single-Pomeron exchange, the BFKL-ladder. As it is well-known, these ladder diagrams are purely imaginary, and they are obtained by simply squaring the $2\to n$ leading-order production amplitudes. In other words, the BFKL-Pomeron is given by the diffractive cut only. The other cuts through the ladder diagrams are down by one or more powers in α_s: the gluon has negative signature, and, to leading order, its signature factor is real. Cutting such a reggeon, therefore, costs one power of α_s, and the multiperipheral or double-multiperipheral cuts will come in only with the next-to-leading order corrections to the BFKL-Pomeron. In order to get to the AGK-rules as closely as possible, we have to define a more precise procedure. First we need a precise definition of what we mean by the "two-reggeon exchange" in the elastic scattering amplitude. Since we would like to satisfy, as much as possibe, unitarity on both the direct and cross channel, we have to start from those kinematic regions where unitarity applies, i.e. from the discontinuities in both s and t. In the high energy limit, t-channel unitarity is expressed in terms of reggeon unitarity equations; it is therefore natural to take the discontinuity of the partial wave across the cut in the angular momentum plane, and to move to the branch point of this cut. Ignoring, for the time being, all problems connected with the infrared divergence of the gluon trajectory function, the discontinuity is given by the following reggeon unitarity equation (Fig.5.1):

$$\begin{aligned} disc_j F(j,t) \;&=\; \frac{1}{i}\left[F(j_-,t)-F(j_+,t)\right] \\ &=\; \frac{1}{2}\int\frac{d^2k}{(2\pi)^3}C_2(\omega_+;k,q-k)\frac{2\pi\delta(\omega+2-\alpha(k^2)-\alpha((q-k)^2))}{k^2(q-k)^2}C_2(\omega_-;k,q-k). \end{aligned} \tag{5.2}$$

Here C_2 is the amputated counterpart of D_2 (cf.(4.1)). As we said before, this contribution to the partial wave is positive and comes from the diffractive cut alone: the propagators $1/k^2$ and $1/(q-k)^2$ are the (real- valued) signature factors of the gluons to the right or the left of the cutting line, and to cut one of them costs one power of α_s. One has therefore to expect that reggeon unitarity equations with a cut gluon should arise once we consider the correction to the BFKL Pomeron.

Now we apply the same arguments to the diagrams of Fig.5.2 which contain, among other contributions, the two-Pomeron cut. On the one hand, we could begin with our results obtained in the previous sections: starting from the partial wave for the $3 \to 3$ amplitude illustrated in Fig.4.1, we take the discontinuities across the two-reggeon cuts in the two lower t-channels and integrate over M^2: this leads to the partial wave amplitude D_4. The discussion of the previous section has shown that it is not the full D_4 which defines the two-Pomeron cut: we first have to take out the reggeizing terms D_4^R which appear to play a special role. Following this experience our ansatz for the two-Pomeron cut in the reggeon unitarity equations becomes:

$$disc_j F(j,t) = const \int \prod_i \frac{d^2k_i}{(2\pi)^3} \delta^{(2)}(\sum_i k_i) \; C_4^I(\omega_+; k_1, ..., k_4) \frac{2\pi\delta(\omega + 4 - \sum_i \alpha(k_i))}{k_1^2 ... k_4^2} C_4^I(\omega_-; k_1, ..., k_4), \qquad (5.3)$$

where, in the partial waves C_4^I, the (12) and (34) systems are in even signature state (e.g. the color singlet state). For the exchange of two even-signature states with a singularity close to unity we know from general Regge theory (see, for example, [18] or [19]) that there is a negative constant in front of the unitarity equation: $const = -\frac{\pi^2}{2}$. This way of proceeding may be viewed as being more "t-channel" oriented, since it uses the t-channel unitarity equations (in the form of reggeon unitarity) for obtaining the two Pomeron contribution to the elastic scattering amplitude.

The nontrivial task now is to show that the same result is obtained from s-channel unitarity, i.e. by summing over different contributions on the rhs of eq.(5.1). Moreover, if the AGK rules are to be valid, the diffractive, single-multiperipheral and double-multiperipheral contributions should come with very specific relative weights. The rhs of (5.1) is illustrated in Fig.5.3. Whereas for the leading approximation, the BFKL-Pomeron, the $T_{2\to n}$ on the rhs have been taken in the leading-ln s approximation, we now need corrections to the production amplitudes. In the first term of Fig.5.3, they are imaginary and given by diagrams with one or two gluons in the t-channel; these amplitudes have first been discussed in [16]. In the second term of Fig.5.3 one sees amplitudes with three gluons in the t-channel: they are real-valued, and first examples have been discussed in [16]. In general, the analysis of production amplitudes is rather involved: one has to study all signature configurations seperately, and each amplitude has several independent partial waves. Studies contained in the papers mentioned, however, indicate that the results can be summarized in a rather simple way. For example, for each production amplitudes with two gluons in the t-channel which contributes

to Fig.5.3a, the sum over all signatures and all independent partial waves can be written as a multiple Mellin integral over all subenergies, and the transform which depends upon several angular momentum variables can be written down in terms of simple rules. Instead of signature factors, we have a simple $2\pi i$, and factor $1/2!$ takes care of statistics. Similarly, for production amplitudes with a three-gluon t-channel state which contribute to Fig.5.3b,c the signature factors are replaced by a factor $-(2\pi)^2$, and the statistics factor is $1/3!$. As a result of these rules, we can write down the expressions for any diagram in Fig.5.3, if we use the rules listed in the beginning of section 4 and multiply by the contants $(2\pi)^2/2!2!$, $-(2\pi)^2/3!$ for Fig.5.3a and Fig.5.3b, resp.

The further analysis of these diagrams proceeds in the same way as for the BFKL ladders: again we shall investigate only the vicinity of the singularites in the complex angular momentum plane by taking the discontinuity across the four-reggeon cut. Apart from the constants mentioned before, it has the form (5.3). Then we make use of our analysis of D_4 in the previous section and decompose our expressions into various different contributions.

We begin with the first term in Fig.5.3; the constant in (5.3) turns out to be $2\pi/2^2$. Next we write C_4 as a sum of two terms (cf.(4.1)):

$$C_4 = (D_4^R + D_4^I)(\omega + 4 - \sum_i \alpha(k_i)), \qquad (5.4)$$

and our reggeon unitarity equation becomes a sum of four terms. The first of them is obtained by chosing the reggeizing terms D_4^R both above and below the unitarity cut. According to the decomposition (2.9) (which in the previous section has been shown to be correct to all orders), this contribution comes as a sum of many terms; a few examples are shown in Fig.5.4. The most interesting ones are the "diagonal" ones (Fig.5.4a - c) where the reggeization schemes above and below match. Altogether, there are seven terms of this type, and together with the s-channel cutting line they have quite different interpretations. Let us begin with the first one (Fig.5.4a). Because of the "reggeon-cut" killing factor in (5.4), the discontinuity across the four-reggeon cut in the angular momentum plane vanishes. We therefore have to move to the other singularities connected with the four-gluon t-channel state. A careful analysis which will not be described here in detail (see [17]) shows that this are, simultaneously, the two-particle singularities in the t_{12} and the t_{34} channels and the two-reggeon cut generated by $\alpha(t_{12})$ and $\alpha(t_{34})$. Our unitarity integral therefore describes, in both these subchannels, the two-particle contribution to the gluon trajectory function. By writing dispersion relations in t_{12} and t_{34}, Fig.5.4a can be read as " Fig.5.1 $\cdot(\beta(t_{12}) \cdot \beta(t_{34}))$ ". Including now also the s-cut line, Fig.5.4 is interpreted as the "diffractive" cut of a two-reggeon contribution. Taking into account the color structure of (2.9) we have to distinguish between two different types of two-reggeon states. The first one belongs to the f-part in (2.9), and it provides a higher order correction to the BFKL ladders (the order α_s correction to the signature factors of both gluons). The second one is due to the corresponding d-terms in (2.9), and it gives, for the even-signature 8_S reggeon, the diffractive cut. In contrast to the 8_A gluon case where the diffractive cut is leading compared to the other cuts, this even-

signature reggeon has the same features as the Pomeron: all cuts are of the same order. The next class of terms (Fig.5.4b) are "double multiperipheral" cuts: they represent the expected contributions mentioned before, both for the 8_A and the 8_S reggeon. The remaining terms belong to the three-particle contribution to the gluon trajectory function (Fig.5.4c) and are new. The "nondiagonal" pieces, finally, are interpreted as "cut vertices" (Fig.5.4d), i.e. higher oder corrections to the four-reggeon interaction vertex for which the BFKL-kernel represents the lowest-order term.

Next the mixed terms of the type $C_4^R...C_4^I$. Again, we have a "reggeon-cut killing factor" from C_4^R above and move on to the four-gluon particle cut. Because of the complete symmetry of the vertex V in C_4^I (3.11) which is preserved by the subsequent pairwise interactions between the gluons, there is no coupling of C_4^I to any of the f-terms in C_4^R (cf.(4.3)) , i.e. no transition of the type 8_A reggeon $\rightarrow$ two 8_A reggeons, in agreement with the signature conservation rules. What remains, are either transitions of the type 8_S reggeon $\rightarrow$ two 8_A reggeons or 8_A reggeon $\rightarrow$ three 8_A reggeons. Our unitarity analysis yields discontinuities in the t-channel, and we have to use a dispersion integral to calculate the full vertices, e.g.the $8_S \rightarrow$ two 8_S reggeon vertex. Details of this argument will be presented elsewhere.

Finally we consider the terms of the type $C_4^I...C_4^I$. Following [9] it useful to cast the C_4^I into a somewhat different form. We start from (4.5) which we write as

$$D_4^I \;=\; \frac{1}{\omega} D_2 \otimes V + D_4^I \otimes \sum \frac{K_{2\rightarrow 2}+\alpha-1}{\omega} \;. \tag{5.5}$$

In the kernel the sum goes over all pairs (ij) of gluon lines, and the combination of kernels and trajectory functions is such that infrared divergencies cancel ([9]). The formal solution to this equation is given in (4.13). As an alternative to this, we define the auxiliary potentials $\tilde{T}_{(12)(34)}$, which represents the sum over all pairwise interactions between gluon 1 and 2 or gluon 3 and 4 (at least one interaction). In the same way we introduce $\tilde{T}_{(13)(24)}$, and $\tilde{T}_{(14)(23)}$. Next we define the three amplitudes $T_{4\,(12)(34)}$, $T_{4\,(13)(24)}$, and $T_{4\,(14)(23)}$ through the integral equations

$$\begin{pmatrix} T_{(12)(34)} \\ T_{(13)(24)} \\ T_{(14)(23)} \end{pmatrix} = \begin{pmatrix} \tilde{T}_{(12)(34);0} \\ \tilde{T}_{(13)(24);0} \\ \tilde{T}_{(14)(23);0} \end{pmatrix} + \begin{pmatrix} \tilde{T}_{(12)(34)} & 0 & 0 \\ 0 & \tilde{T}_{(13)(24)} & 0 \\ 0 & 0 & \tilde{T}_{(14)(23)} \end{pmatrix} \cdot \begin{pmatrix} 0 & 1 & 1 \\ 1 & 0 & 1 \\ 1 & 1 & 0 \end{pmatrix} \begin{pmatrix} T_{(12)(34)} \\ T_{(13)(24)} \\ T_{(14)(23)} \end{pmatrix} . \tag{5.6}$$

Our function D_4^I can then be written as

$$\begin{aligned} D_4^I \;&=\; \frac{1}{\omega} D_2 \otimes V \;+\; D_2 \otimes V \otimes \left(T_{(12)(34)} + T_{(13)(24)} + T_{(14)(23)} \right) \\ &=\; D_{4\,(12)(34)} + D_{4\,(13)(24)} + D_{4\,(14)(23)} . \end{aligned} \tag{5.7}$$

A similar decomposition holds for the "amputated" functions C_4^I. As to the group structure, it is convenient to form irreducible representations of the two-gluon systems. For example, for

$T_{(12)(34)}$ it is natural to consider the color quantum numbers of the (12) and (34) subsystems. This introduces, at each switch from one set of systems to another, a 5×5 color recoupling matrix which is given in the appendix of [9] and will not be needed here. With this decomposition (5.7) we now go into the unitarity equation (5.3) and obtain the three terms shown in Fig.5.5 (note that the "nondiagonal" contributions are taken care of if we define the ladders above and below the t-cut to include zero rungs). Because of the symmetry of the transition vertex V, all three terms give identical contributions. With the s-cutting line being included, the interpretation is straightforward: the first term belongs to the diffractive cut, the other two to the double multiperipheral one.

It remains to repeat this analysis for the other contributions in Fig.5.3. Apart from the overall coefficients, only the position of the s-cut changes. As an example, we consider the two-Pomeron cut. The diagrams of Fig.5.5 are changed: all three terms now give multiperipheral contributions. Combining all three terms on the rhs of Fig.5.3 and by taking only the statistics factors in front of the unitarity integral, the counting is as follows:
(i) diffractive cut: $(1/2)^2 = 1/4$,
(ii) multiperipheral cut: $-3 \cdot 2 \cdot 1/3! = -1$,
(iii) double-multiperipheral cut: $2 \cdot (1/2)^2 = 1/2$.
This is in full agreement with the AGK-cutting rules.

This analysis shows that the reggization pieces in D_4 play a very important role. First, they give the nonleading cuttings of the BFKL-Pomeron which are predicted by the AGK-rules for odd-signature reggeons (there also new contributions, e.g.the three-particle state in the gluon trajectory function, the 8_S reggeon, and cut four reggeon vertices). Secondly, only after the subtraction of these reggeizing terms from the four gluon amplitude we found the symmetric vertex V which was needed to arrive at the correct AGK-counting.

6 Summary and Discussion

In this paper we have calculated, within perturbative QCD, the cross section for the diffractive dissociation of a virtual photon in deep inleastic scattering in the triple Regge limit $s \gg M^2 \gg Q^2 \gg \Lambda^2$. Provided we couple our result to a colorless hadron, the formula for the cross section is infrared finite. The large Q^2 of the photon is what justifies the use of perturbation theory. There is both theoretical and experimental interest in this process. This cross section defines the triple Pomeron vertex which plays a key role in the understanding of the Pomeron: approaching the Regge limit from the low-x region of deep inelastic scattering therefore allows to calculate this vertex in perturbative QCD. The result is quite interesting: the cross section is not simply a product of three BFKL ladders with some vertex connecting them, but the Pomeron "above" the vertex is more "composite" than the two Pomerons "below". It contains, even in this leading approximation, already the state of four (reggeized) gluons which, in an elastic scattering amplitude, appears as a first correction to the BFKL ladder diagrams. Correspondingly, the triple Pomeron vertex consists of several pieces, all

of which appear to be crucial for the AGK cutting rules.

From the experimental point of view the cross section formula may be of interest in connection with the "rapidity gap events" seen at HERA. Although we have not yet attempted to perform a numerical analysis of our formula, a few general comments can already be made. First of all we emphasize the limits of the applicability. The use of perturbation theory is justified by the large photon mass. This large momentum scale will feed into the interior of the diagrams, in particular down to the triple Pomeron vertex and into the lower BFKL Pomerons. Because of the well-known transverse momentum diffusion, however, also the region of small transverse momenta contributes: we expect that, inside the diagrams, its role becomes the more important the further we move away from the large-mass photon at the top. Consequently, the kinematics in the vicinity of the triple Pomeron vertex may already be rather strongly influenced by medium or small momenta; it therefore may be necessary to impose a cut on the transverse momenta of those jets which are closest to the "rapidity hole". As an alternative, one may think of a phenomenological improvement of our perturbative calculation in the region of small momenta - similar to the treatment contained in [20].

A second important restriction applies to the missing mass M^2. Apart from the lowest-order calculation of the $q\bar{q}$ final state, our formula is valid only in the region of sufficiently large M^2: this is the region where gluon exchange in the t-channel becomes dominant. For not so large M^2 another approximation contained in [7] has to be used; it is, however, limited to the leading Q^2 approximation and neglects the interaction of the two ladders below the triple Pomeron vertex.

Finally we would like to discuss the implications of our results for the Pomeron structure function [21]. The concept of the Pomeron structure function views the Pomeron as an "incoming particle" on which the photon scatters inelastically. This assumption includes the factorization of the cross section into a Pomeron flux factor which is independent of $x_{Bjorken}$ and Q^2 and the Pomeron structure function. The latter is expected to satisfy the momentum sum rule $\int_0^1 dzzg_{Pomeron}(z) = const$, and its evolution in Q^2 is assumed to follow the usual GLAP evolution equation. In the case of hadron-hadron scattering is has been pointed out [22] that factorization fails for hard diffractive events. The reason for this is the possibility of exchanging a soft gluon across the hard production subprocess. In the case of photon diffractive dissociation this mechanism does not work, since the exchange of gluons is controlled by the hard scale Q^2. However, it was shown in [7] that the Q^2-evolution equation of this process has its pecularities. The structure function was found to satisfy an inhomogeneous evolution equation where the inhomogeneous term consists of the two lower Pomeron ladders and a triple ladder vertex. It therefore depends upon the momentum scale at the triple ladder vertex, Q'^2, which has to be integrated and receives contributions from both the small and large momentum region. Consequently, there is no strict factorization. Only the neglect of this Q'^2-integration - i.e.the neglect of any scale evolution inside the ladders and the triple ladder vertex - would justify the usual QCD evolution framework for

the Pomeron structure function.

The results of this paper show that the triple-ladder vertex discussed in [7] is imcomplete and the Q^2 evolution is even more complex. Our triple-Regge high energy approximation (leading $\ln(1/x)$, $\ln(M^2/Q^2)$) which includes higher twist contributions demands both two-gluon and four-gluon t-channel states above the branching vertex. As a consequence, the Q^2 evolution above this vertex differs from the usual GLAP evolution which is based upon the two-gluon t-channel state approximation. Although we do not yet have numerical results there is no doubt that the increase in M^2 due to the four gluon state $G_{4\to 4}$ is stronger than that due to the two-gluon state (BFKL Pomeron). At large M^2, therefore, $G_{4\to 4}$ will certainly dominate. For $M^2 \sim Q^2$, on the other hand, the role of $G_{4\to 4}$ may be less significant, but this is far from being obvious. We hope that our formula provides a reliable starting point for investigating this question in more detail.

References

[1] ZEUS Collab. (M.Derrick et al.) DESY-93-110.

[2] H1 Collab. (I.Abt et al.) *Nucl.Phys.***B 407** (1993) 515.

[3] ZEUS Collab. (M.Derrick et al.) *Phys.Lett.* **B 315** (1993) 481.

[4] H1 Collab. (J.Dainton, Talk given at the International Symposium on Lepton and Photon Interactions at High Energies, Cornell, August 1993).

[5] M.G.Ryskin, *Sov. J. Nucl. Phys.***52** (1990) 529.

[6] M.Wüsthoff, Diplomarbeit, Hamburg 1992 (unpublished).

[7] E. Levin, M. Wüsthoff, preprint DESY 92-166 (1992), FERMILAB-Pub-92/334-T (Nov. 1992).

[8] N.N. Nikolaev, B.G. Zakharov, *Zeitsch. Phys.* **C53** (1992) 331.

[9] J.Bartels, *Phys.Lett.***B 298**(1993) 204; *Zeitschr.f.Physik***C 60** (1993) 471.

[10] V.A.Abramovsky, V.N.Gribov, O.V.Kancheli, *Sov.Journ.Nucl.Phys.***18** (1973) 595.

[11] V.V. Sudakov, *ZhETF***30** (1956) 187.

[12] A.H. Mueller: Nucl. Phys. B335, 115 (1990).

[13] J. Bartels, A. de Roeck, M. Loewe: Z. Phys. C54, 635 (1992).

[14] E. Levin, M. Ryskin: Sov. J. Nucl. Phys. 53, 653 (1991).

[15] E.A. Kuraev, L.N. Lipatov, V.S. Fadin: Sov. J. Nucl. Phys. 44(3), 443 (1976)
and Sov. J. Nucl. Phys. 45(2), 199 (1977),
Ya.Ya. Balitskii, L.N. Lipatov: Sov. J. Nucl. Phys. 28(6), 822 (1978).

[16] J.Bartels, *Nucl.Phys.***B 175**(1980) 365.

[17] J. Bartels: preprint DESY 91-074 (1991).

[18] H.D.I.Abarbanel, J.B.Bronzan, R.L.Sugar, and A.R. White, *Phys.Rep.***C 21** (1975) 119.

[19] A.R.White, *J.Mod.Physics***A11** (1991) 1859; ANL-HEP-PR-93-16.

[20] A.J.Askew, J.Kwiecinski, A.D.Martin, P.J.Sutton, Durham preprint DTP-93-28.

[21] G.Ingelman, P.Schlein, *Phys.Lett.***B 152** (1985) 256.

[22] J.C.Collins, L.Frankfurt, M.Strikman, *Phys.Lett.* **B 307** (1993) 161.

[23] N.N.Nikolaev, B.G.Zakharov, KFA-IKP(Th)-1993-17.

Figure Captions:

Fig.2.1: the diffractive dissociation of the virtual photon into $q\bar{q}$ + and n gluons in the triple Regge limit.

Fig.2.2: the six-point amplitude $T_{3\to 3}$.

Fig.2.3: the lowest order diagrams of the diffractive dissociation $\gamma + q \to q\bar{q} + q$.

Fig.2.4: a) the lowest order diagrams of the process $\gamma + q \to q\bar{q} + q$ with single gluon exchange. b) the square of the matrix element leading to $D_{(2;0)}$ in (2.4). Only the first two box-diagrams contribute whereas the third belongs to the left hand cut in the invariant mass of the two-fermion system.

Fig. 2.5: a more detailed diagram illustrating eq. (2.6). It is the first diagram of Fig.2.3 completed by its crossed counterpart.

Fig.2.6: the reggeization of the gluon. In this type of diagram, a reggeon diagram, the wavy vertical lines denote reggeons, and the straight lines at the bottom, which originally were gluons, stand for the propagators $1/k_{1t}^2$ and $1/k_{2t}^2$.

Fig.2.7: the triple-energy discontinuity of one of the 16 lowest order diagrams.

Fig.2.8: the final set of Regge diagrams contributing to $D_{(4;0)}$ in eq. (2.9). The four gluons have reggeized into two reggeons which couple to the fermion box in exactly the same way as two elementary gluons do (Fig.2.4.b).

Fig.2.9: graphical representation of the colour tensor of the fermion loop with four gluons. The bubble without arrow includes two contributions related to each other through charge conjugation.

Fig.2.10: the quark-antiquark colour decomposition into irreducible singlet and octet colour states.

Fig.2.11: two possible colour representations of the four gluon tensor $d^{a_1a_2a_3a_4}$. The dots and open circles denote the usual f- and d-tensors, resp. (see eq. (2.10)).

Fig.2.12: a reggeon made up of three gluons. It contains both odd and even signature.

Fig.3.1: the complete set of diagrams with single gluon exchange including the emission of one real gluon. The set of effectively contributing diagrams depends on the gauge. We use the physical lightcone gauge with the gauge condition $p \cdot A = 0$.

Fig.3.2: the "effective" production vertex ("Lipatov" vertex). The first diagram in this figure is the combination of the first three diagrams in Fig.3.1 and defines the effective production vertex as given in eq. (3.6). From now on all vertices describing the emission of s-channel gluons from reggeon lines are understood to be effective production vertices.

Fig.3.3: two gluon exchange in the leading $\log(s/M^2)$ approximation. The two gluons reggeize and form the same set of diagrams as in Fig.3.1.

Fig.3.4: some of the Feynman diagrams may be cut in two different ways as illustrated in this figure. Each cut contributes to the discontinuity in s_1. More explanations are given in the text.

Fig.3.5: the cut diagrams may be rearranged in such a way that they combine into reggeon diagrams with effective production vertices (one example is shown here).

Fig.3.6: complete set of Regge diagrams contributing to the production amplitude of the diffractive dissociation $\gamma + q \to q\bar{q} + g + q$.

Fig.3.7: virtual corrections to the diffractive dissociation into the quark-antiquark pair. The bubble in the second and third diagram denotes the Regge trajectory function (eq. (3.7)).

Fig.3.8: complete set of diagrams contributing to the M^2-integrated cross section of diffractive dissociation. The sum in the third term of the first line is meant to include also the square of diagrams in Fig.3.7. In the second line of this figure the reggeizing properties of the lowest order fermion loop ($D_{(3;0)}$ and $D_{(4;0)}$) are indicated.

Fig.3.9: graphical illustration of the kernels in eq. (3.8).

Fig.3.10: colour structure of the first diagram in Fig.3.8 and its reduction to elementary colour tensors.

Fig.4.1: the triple-energy discontinuity which determines the partial wave in eqs.(2.1) and (2.2).

Fig.4.2: the coupled integral equations for the reggeon amplitudes D_2, D_3, and D_4. The sum in the second and third equation refers to the permutations of gluon lines.

Fig.4.3: graphical illustration of the two Green's functions used eqs.(4.14) and (4.16).

Fig.4.4: diagrammatic illustration of the diffractive dissociation cross section. The reggeon diagrams on the rhs inside the brackets are amputated, i.e. there is no enrgy denominator for the gluon lines at the bottom. The prime at the summation symbol in the first line indicates that sum over all gluon pairings is incomplete: the interaction between the lines 1 and 2 and between the lines 3 and 4 is to be left out.

Fig.4.5: diagrmmatic illustration of eq.(4.16).

Fig.5.1: reggeon unitarity equation across the two-gluon cut.

Fig.5.2: reggeon unitarity equation for the discontinuity across the four-gluon cut.

Fig.5.3: reggeon unitarity equations for different contributions to the energy discontinuity.

Fig.5.4: illustration of Fig.5.3a, with C_4^R both in the upper and lower blob. Further explanations are found in the text (after eq.(5.4)).

Fig.5.5: illustration of Fig.5.3a, with C_4^I both in the upper and lower blob. C_4^I is decomposed according to (5.7), and the crosses in the center of (a) indicate that we are sitting on the leading angular plane singularity of the subsystems (12) and (34). In (b) and (c), the diagrams are nonplanar. Inserting finally the s-cut line leads to the conclusion that (a) belongs to the diffractive cut, (b) and (c) to the double-multiperipheral cut.

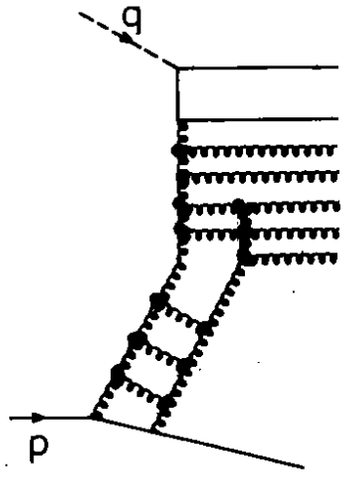

Fig.2.1

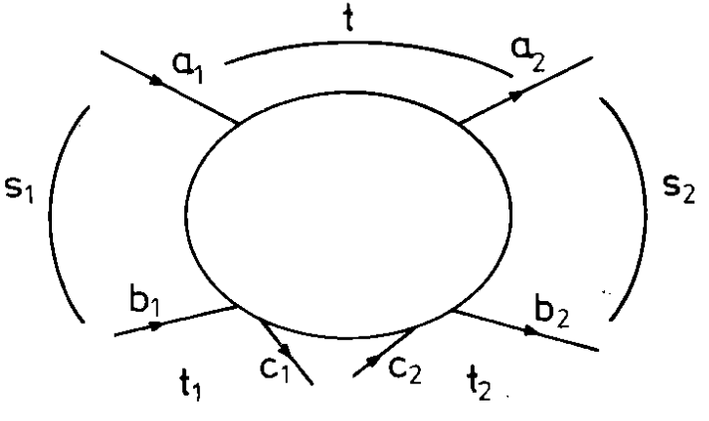

Fig. 2.2

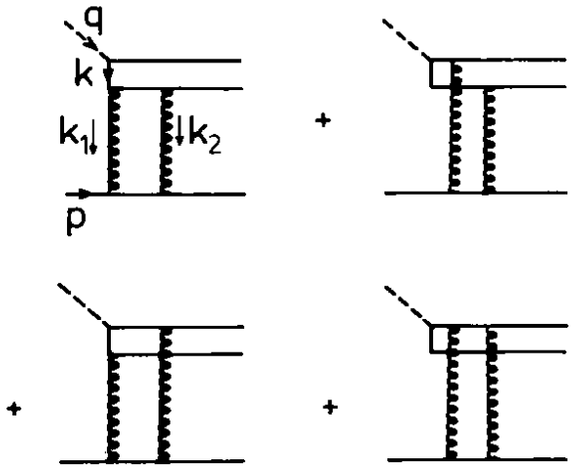

Fig. 2.3

a)

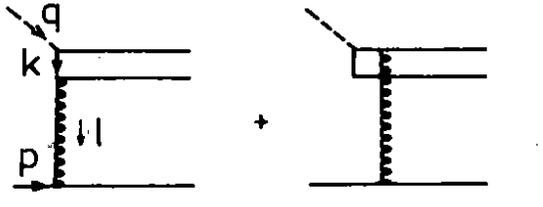

b)

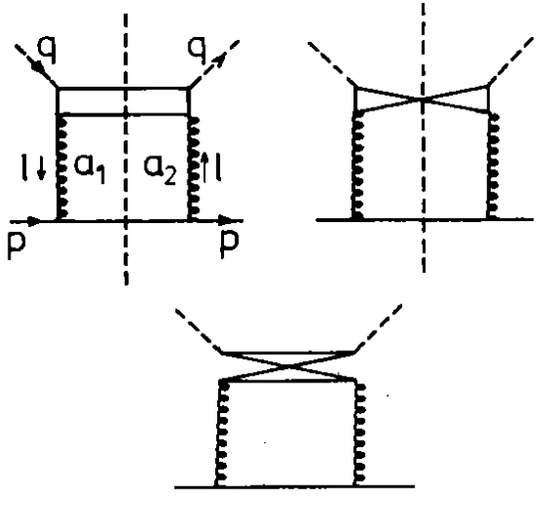

Fig. 2.4

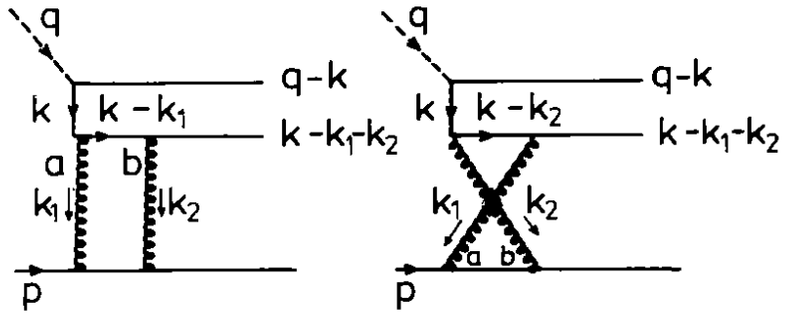

Fig. 2.5

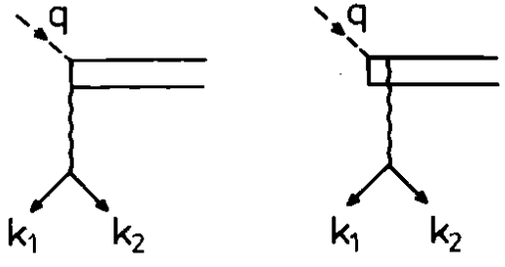

Fig. 2.6

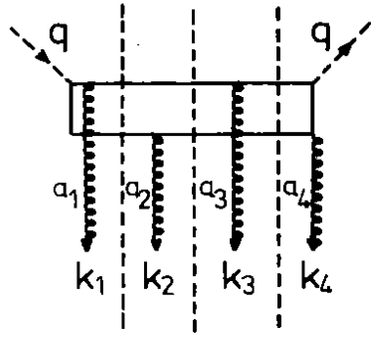

Fig. 2.7

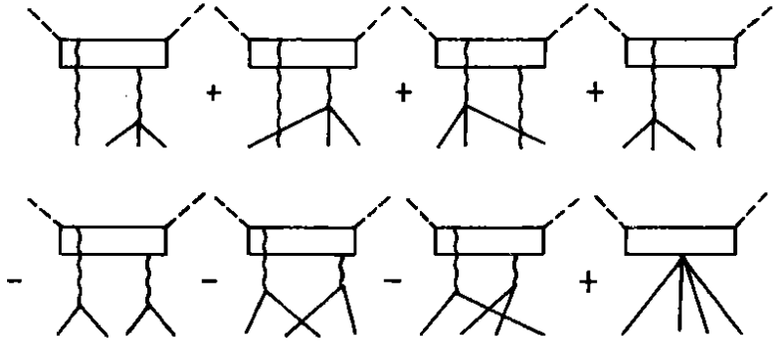

Fig.2.8

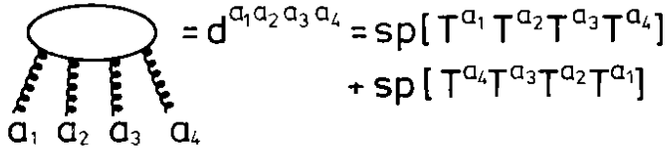

Fig.2.9

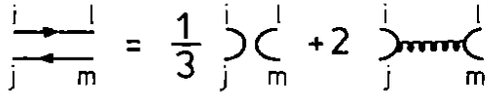

Fig. 2.10

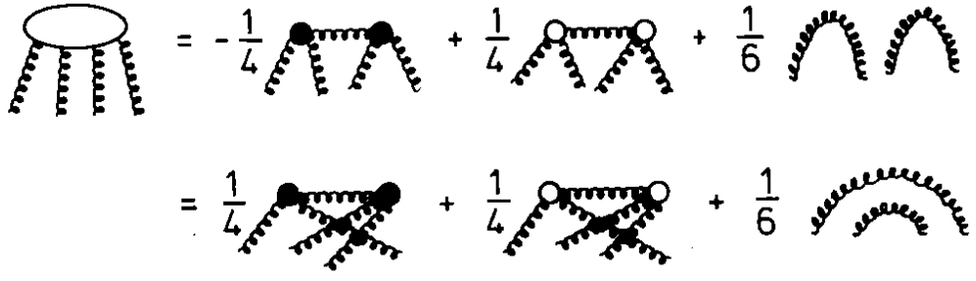

Fig. 2.11

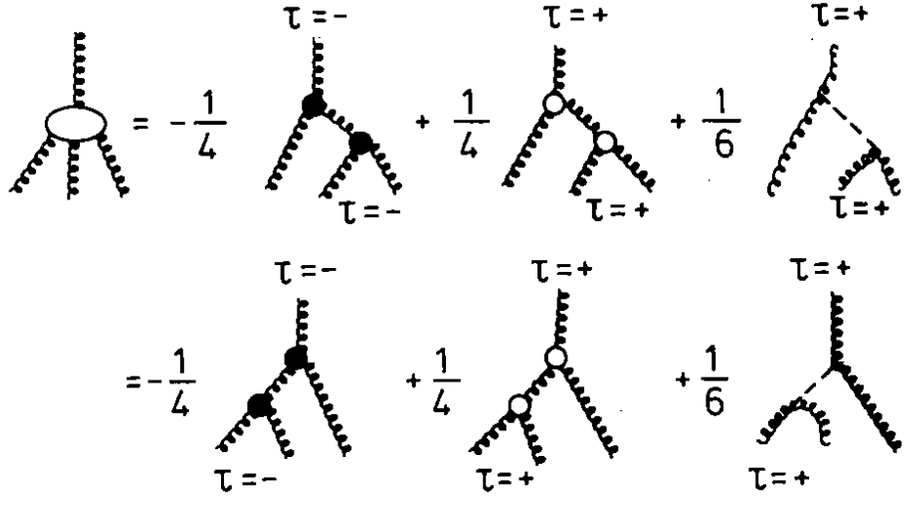

Fig. 2.12

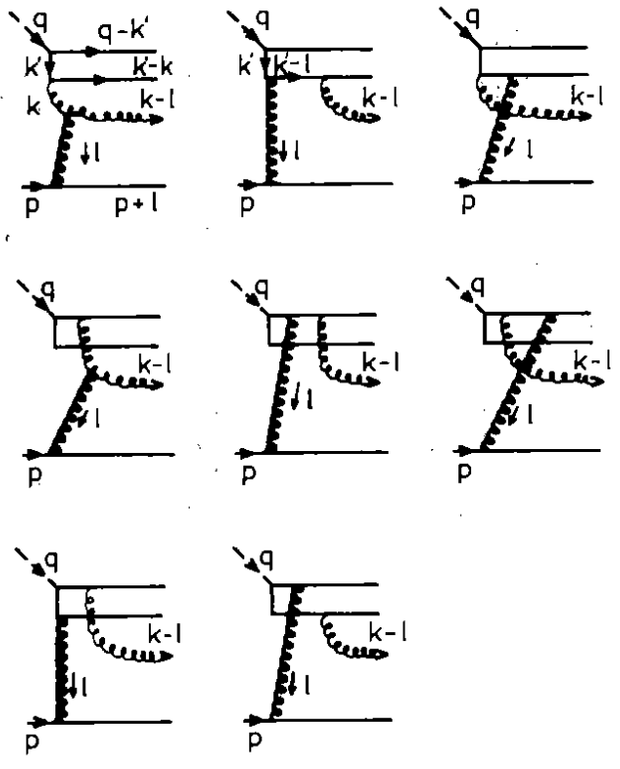

Fig. 3.1

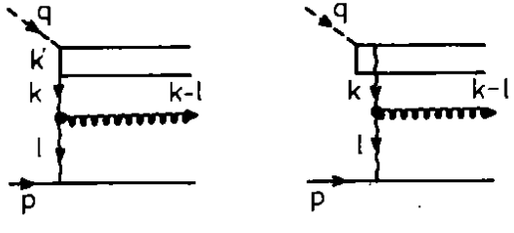

Fig. 3.2

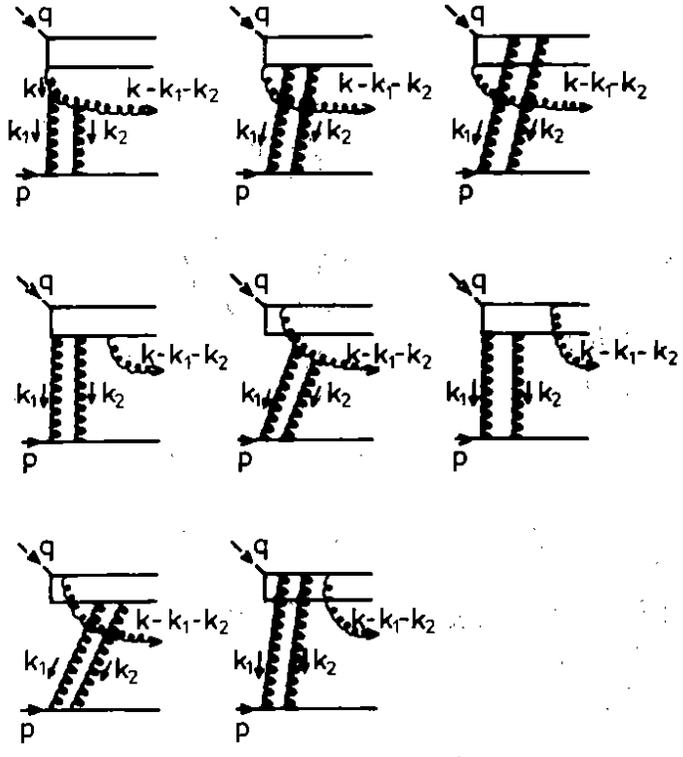

Fig. 3.3

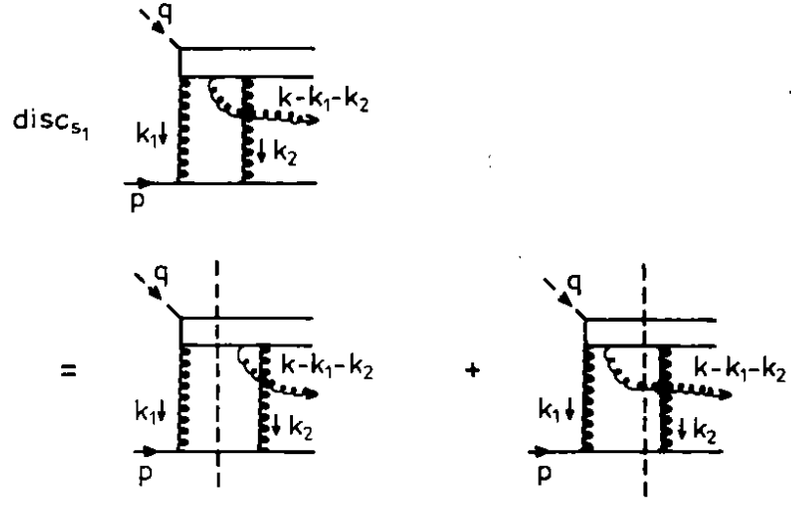

Fig. 3.4

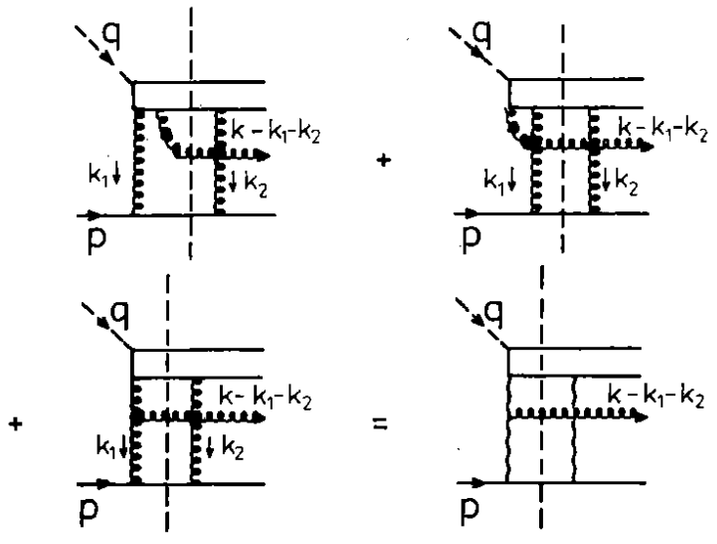

Fig. 3.5

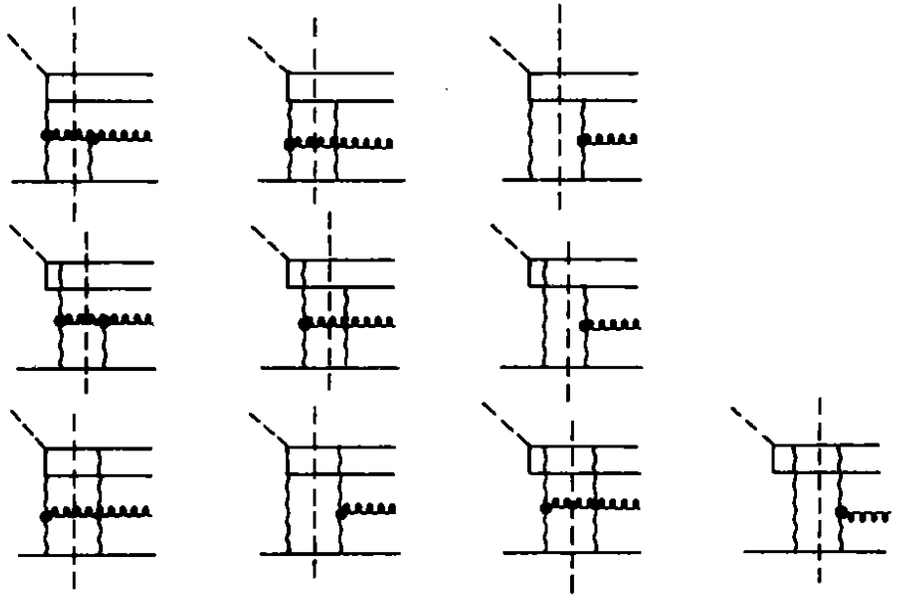

Fig. 3.6

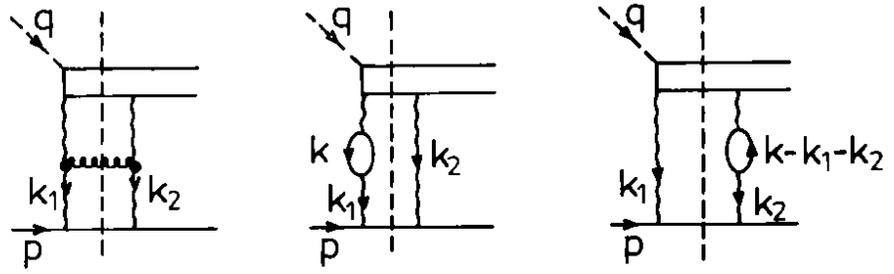

Fig. 3.7

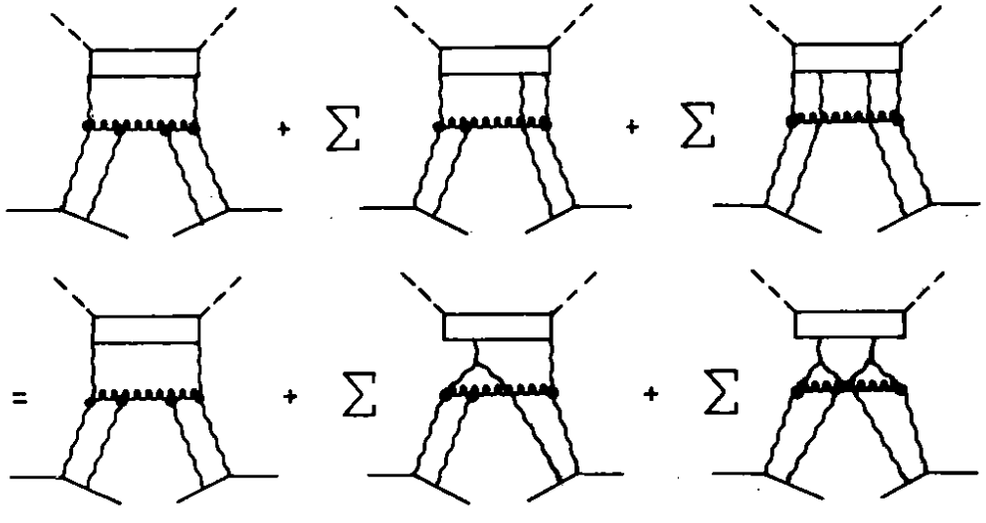

Fig. 3.8

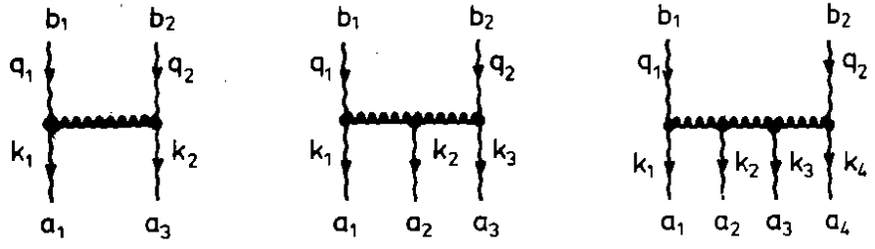

Fig. 3.9

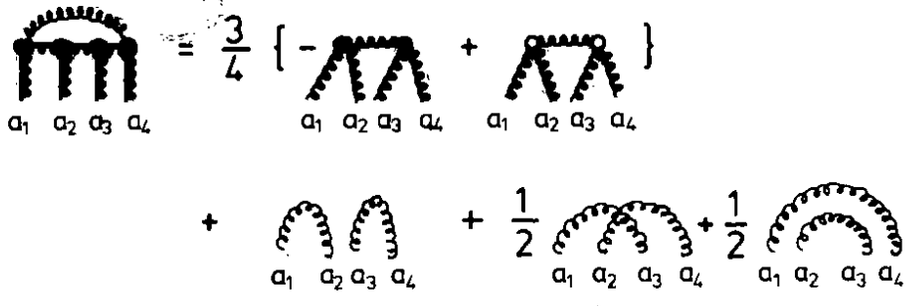

Fig. 3.10

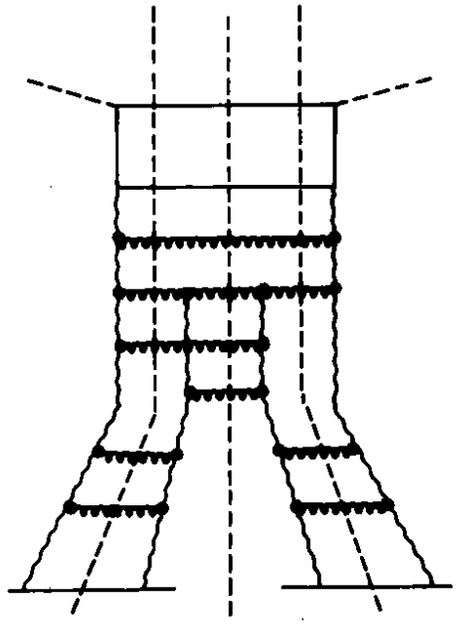

Fig. 4.1

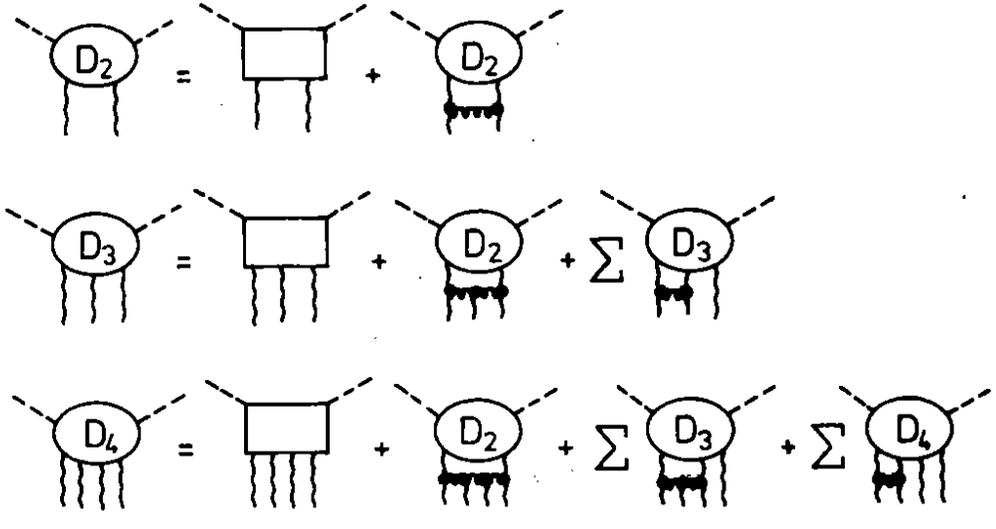

Fig. 4.2

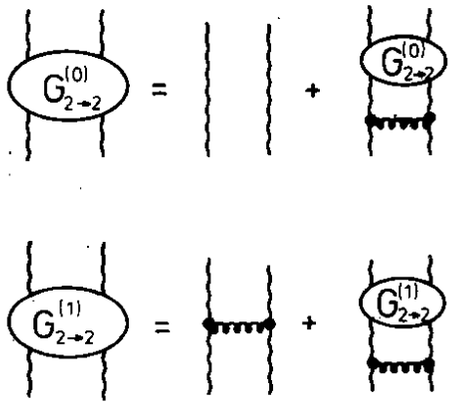
$G^{(0)}_{2\to 2}$ = + $G^{(0)}_{2\to 2}$
$G^{(1)}_{2\to 2}$ = + $G^{(1)}_{2\to 2}$

Fig. 4.3

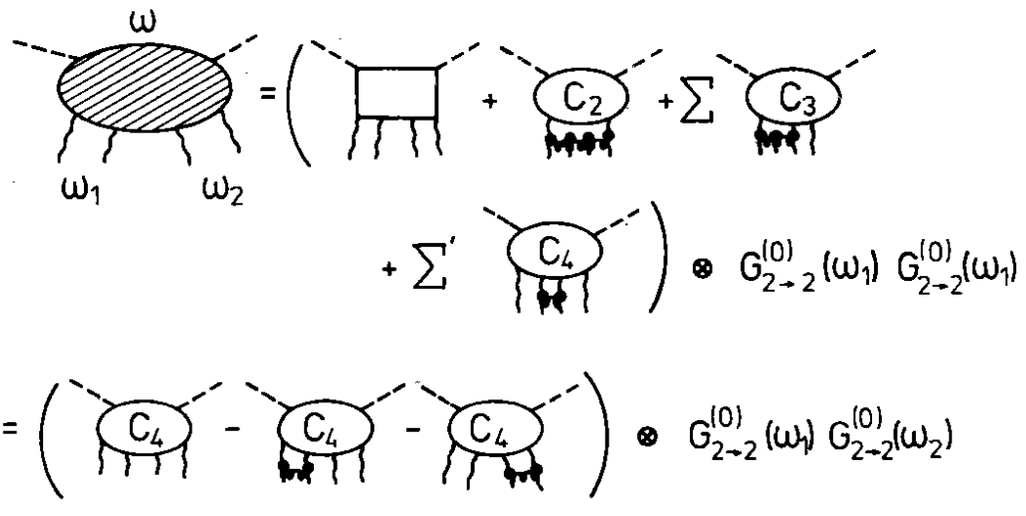
ω
ω_1
ω_2
= (+ C_2 + ∑ C_3
+ ∑′ C_4) ⊗ $G^{(0)}_{2\to 2}(\omega_1)$ $G^{(0)}_{2\to 2}(\omega_1)$
= (C_4 - C_4 - C_4) ⊗ $G^{(0)}_{2\to 2}(\omega_1)$ $G^{(0)}_{2\to 2}(\omega_2)$

Fig. 4.4

$$\frac{\omega - \omega_1 - \omega_2}{\omega - \sum_{i=1}^{4} \beta_i'}$$

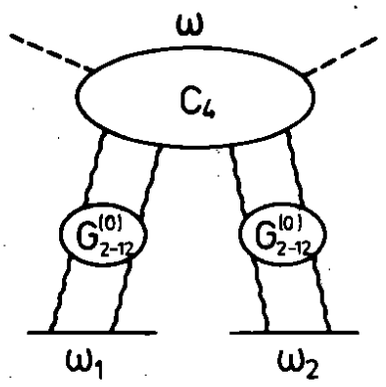

$$= \frac{\omega - \omega_1 - \omega_2}{\omega - \sum_{i=1}^{4} \beta_i'}$$

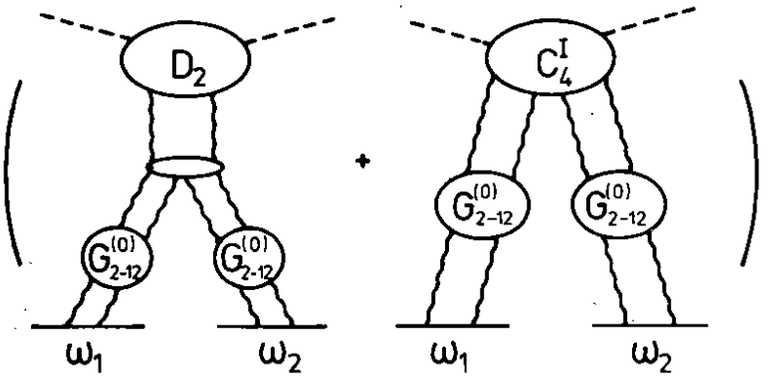

Fig. 4.5

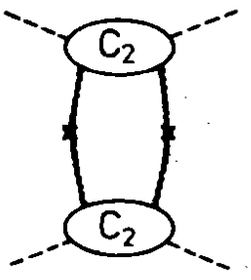

Fig. 5.1

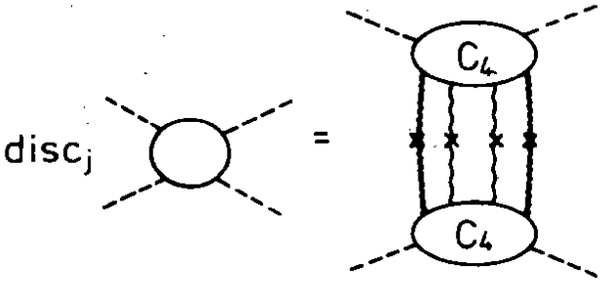

Fig. 5.2

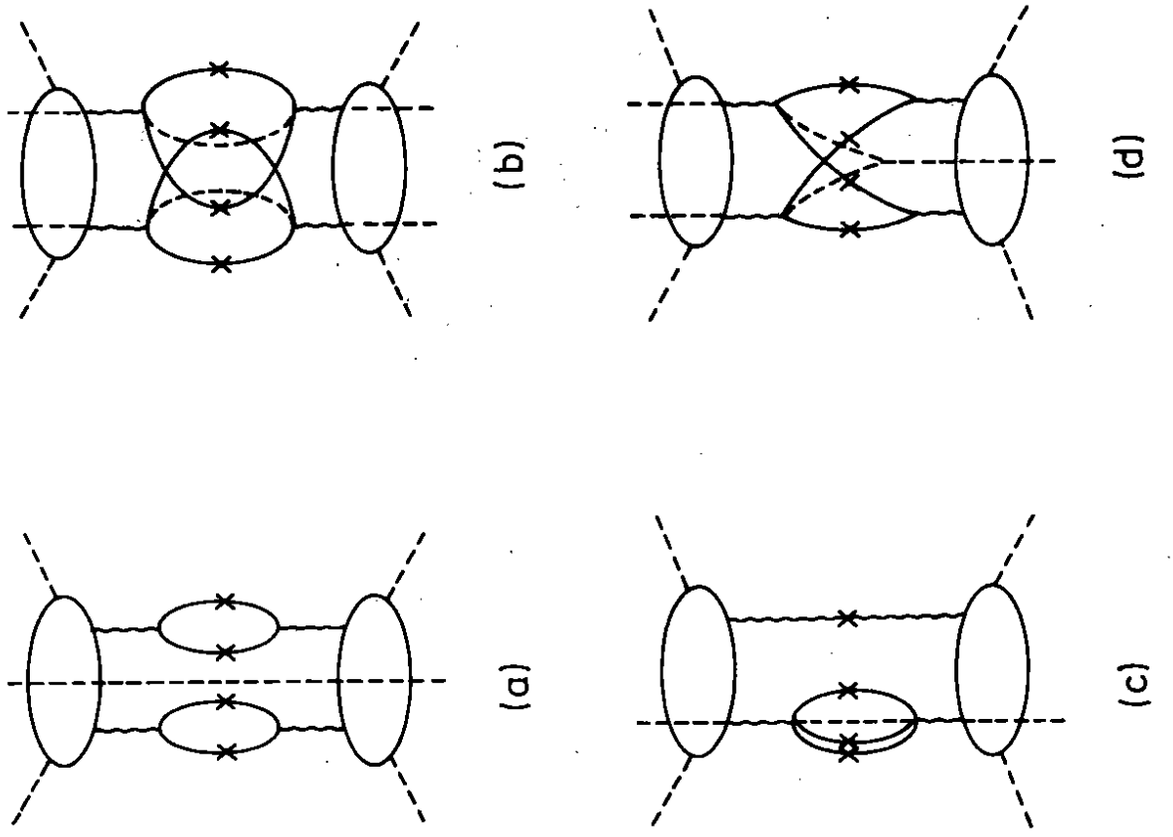

Fig. 5.4

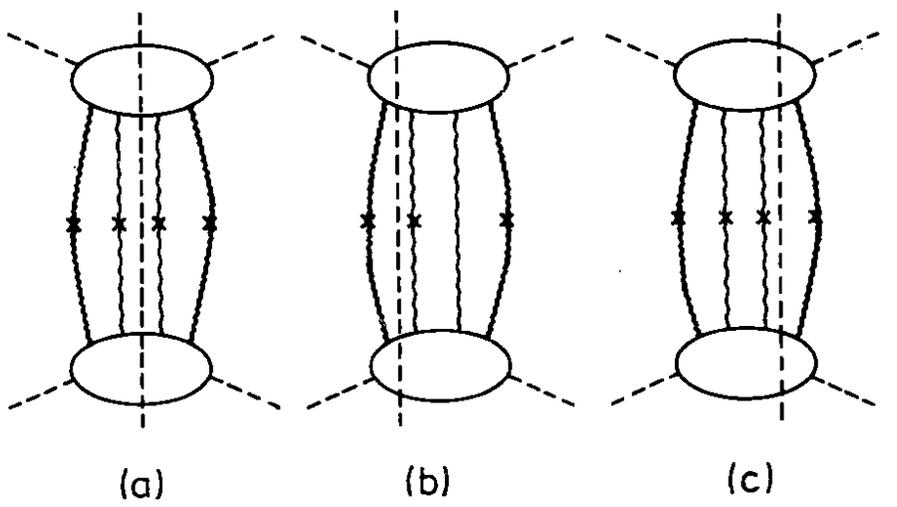

Fig. 5.3

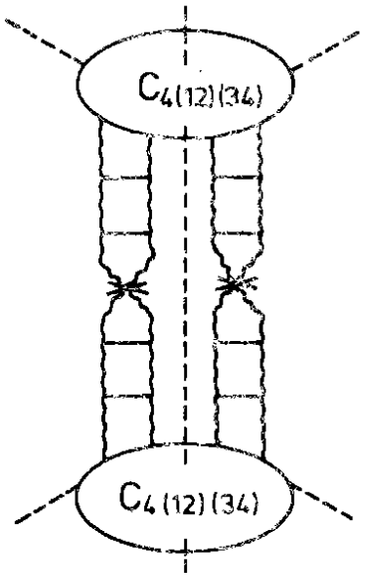

(a)

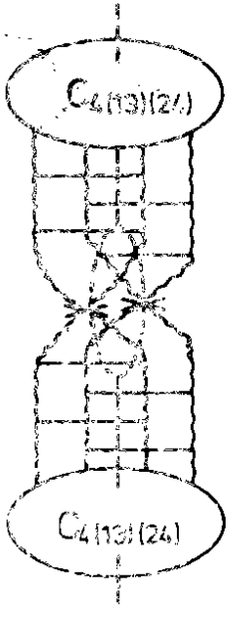

(b)

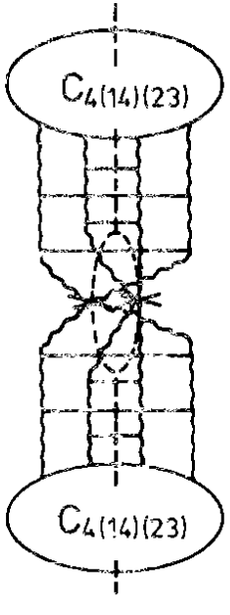

(c)

Fig. 5.5